Table II. *The Candidate proteins and their Syfpeithi scores. Three proteins were analyzed in the following amino acid sequence(†: 966-2920, ‡: 955-2903, §: 1-1669) by Syfpeithi.*

Peptide sequence	Accession No	Protein name	Syfpeithi score		
			A*0201	A*01	A*2402
TKLSA	NP_001034864.2	Absent in melanoma 1-like protein	23	10	
TKLSA	NP_116586.1	Protocadherin-10 isoform 1 precursor	18	14	
TKLSA	NP_065866.1	Protocadherin-10 isoform 2 precursor	18	14	
TKLSA	NP_872579.2	Nucleosome-remodeling factor subunit BPTF isoform 1†	18	11	
TKLSA	NP_004450.3	Nucleosome-remodeling factor subunit BPTF isoform 2‡	18	11	
TKLSA	NP_258260.1	FCH and double SH3 domains protein 1	17	x	
TKLSA	NP_861525.2	Bone morphogenetic protein 8A precursor	14	x	
TKLSA	NP_001711.2	Bone morphogenetic protein 8B precursor	14	x	
TKLSA	NP_938204.2	C-Maf-inducing protein isoform C-Mip	16	22	
TKLSA	NP_085132.1	C-Maf-inducing protein isoform Tc-Mip	16	22	
TKLSA	NP_003491.1	Peroxisomal acyl-coenzyme A oxidase 2	18	15	
TKLSA	NP_997404.1	Reticulon-4 isoform E	18	x	
TKLSA	NP_573400.3	Receptor-type tyrosine-protein phosphatase T isoform 1 precursor	x	x	
TKLSA	NP_008981.4	Receptor-type tyrosine-protein phosphatase T isoform 2 precursor	x	x	
TKLSA	NP_775933.1	RING finger protein 175	17	x	
TKLSA	NP_001697.2	B-cell lymphoma 6 protein isoform 1	11	x	
TKLSA	NP_001128210.1	B-cell lymphoma 6 protein isoform 2	11	x	
TKLSA	NP_004376.2	Versican core protein isoform 1 precursor§	18	x	
TKLSA	NP_001157570.2	Versican core protein isoform 4 precursor	18	x	
TKLSA	NP_005912.1	Mitogen-activated protein kinase kinase kinase 1	18	x	
TKLSA	NP_065393.1	Reticulon-4 isoform A	18	x	
TKLSA	NP_004053.1	Cadherin-16 isoform 1 precursor	25	x	
TKLSA	NP_001191673.1	Cadherin-16 isoform 2 precursor	25	x	
TKLSA	NP_001191674.1	Cadherin-16 isoform 3 precursor	25	x	
TKLSA	NP_001191675.1	Cadherin-16 isoform 4 precursor	25	x	
TKLSA	NP_001035847.1	Serine/threonine-protein phosphatase 4 regulatory subunit 1 isoform a	18	x	
TKLSA	NP_005125.1	Serine/threonine-protein phosphatase 4 regulatory subunit 1 isoform b	18	x	
TKLSA	NP_000316.2	Pituitary homeobox 2 isoform c	22	x	
TKLSA	NP_009058.2	Villin-1	x	x	
TRAGD	NP_001380.2	Down syndrome cell adhesion molecule isoform CHD2-42 precursor	15	x	
TRAGD	NP_005603.3	RE1-silencing transcription factor	14	x	
TRAGD	NP_055400.1	Solute carrier family 40 member 1	x	x	
PARSGA	NP_001073977.1	T-box transcription factor TBX18	15	x	
PARSGA	NP_00101502.1	DNA-3-methyladenine glycosilase isoform b	x	x	
RLRYT	NP_001155250.1	[Pyruvate dehydrogenase (acetyl-transferring)]-phosphatase 1, mitochondrial isoform 1	10	x	x
RLRYT	NP_001155251.1	[Pyruvate dehydrogenase (acetyl-transferring)]-phosphatase 1, mitochondrial isoform 2	14	x	x
RLRYT	NP_060914.2	[Pyruvate dehydrogenase (acetyl-transferring)]-phosphatase 1, mitochondrial isoform 3 precursor	14	x	x
RLRYT	NP_001193981.1	Transmembrane protein 191C	24	x	10
RLRYT	NP_001229242.1	Transmembrane protein 191B	24	x	10
RLRYT	NP_001007126.1	Uncharacterized protein C20orf201	16	x	x
SMLAER	NP_060354.4	PIN2/TERF1-interecting telomerase inhibitor 1	12	x	x

phenotype. Among non-cancerous tissues, only testicular tissue commonly expressed the three identified proteins. Cancer-testis antigen is a well-known cancer-associated molecule of which 8- or 9-mer antigenic peptide presented on HLA molecules is recognized by specific CTLs (24, 25, 26). Various kinds of transiently-expressed genes during spermatogenesis are found in testicular and cancerous tissues (27). Melanoma-associated antigens (28) and cancer/testis antigen-1B (NY-ESO-1) (29) are representative cancer-testis antigens and potential targets of cancer immunotherapy. Thus, it might be conceivable that the three proteins identified in this study might belong to the cancer-testis

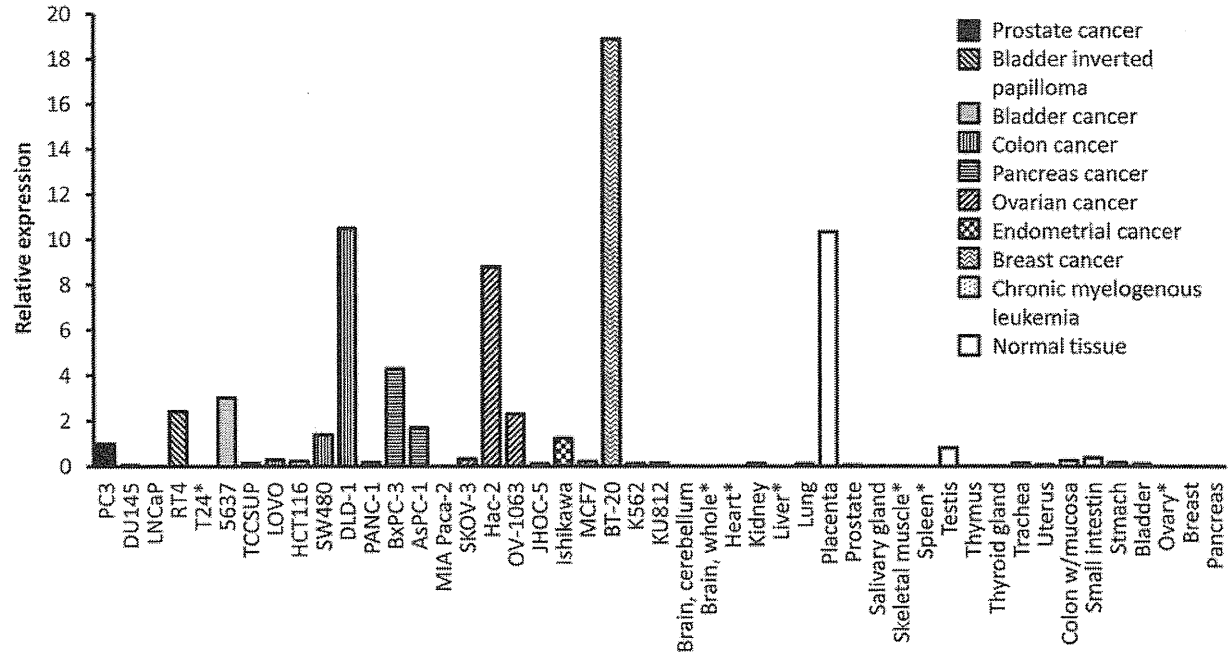

Figure 1. *Expression of absent in melanoma 1-like protein (AIM1L) mRNA in various cancer cell lines and normal tissues. Expression of mRNA encoding AIM1L was analyzed using quantitative reverse transcription-polymerase chain reaction and comparative Ct methods. Each mRNA expression was represented as a value to relative PC3 expression. *Not detected.*

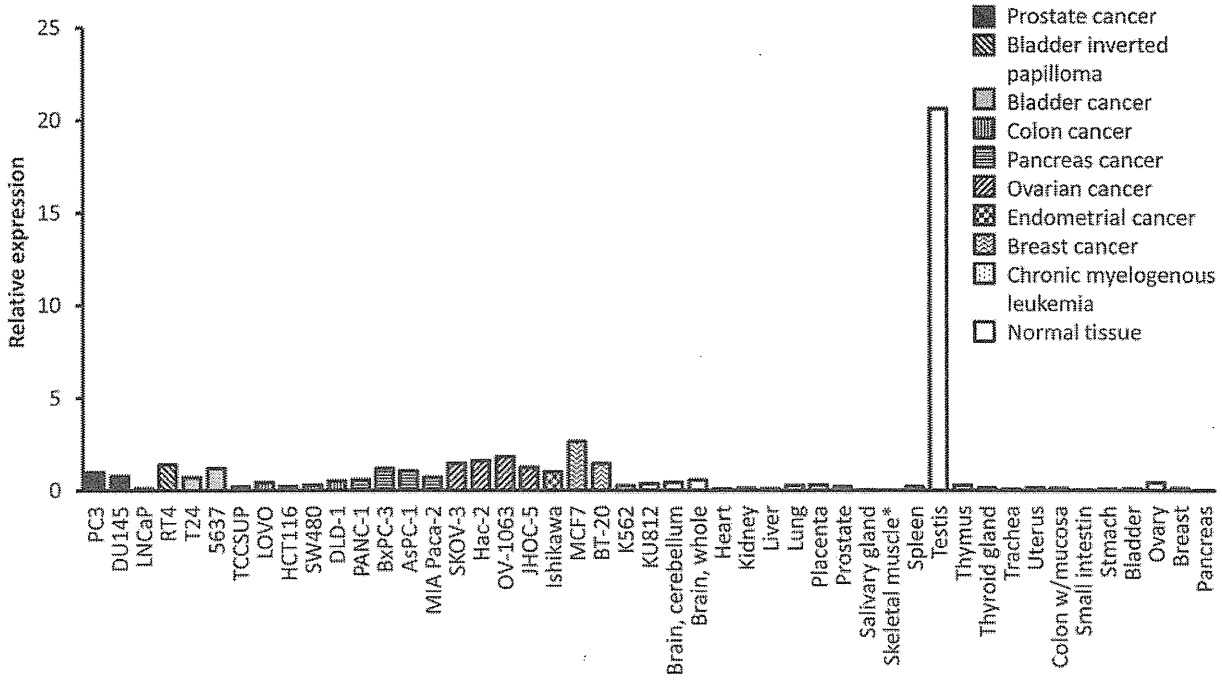

Figure 2. *Expression of trans-membrane protein-191C (TMEM191C) mRNA in various cancer cell lines and normal tissues. Expression of mRNA encoding TMEM191C was analyzed by quantitative reverse transcription-polymerase chain reaction and comparative Ct methods. Each mRNA expression was represented as a value to relative PC3 expression. *Not detected.*

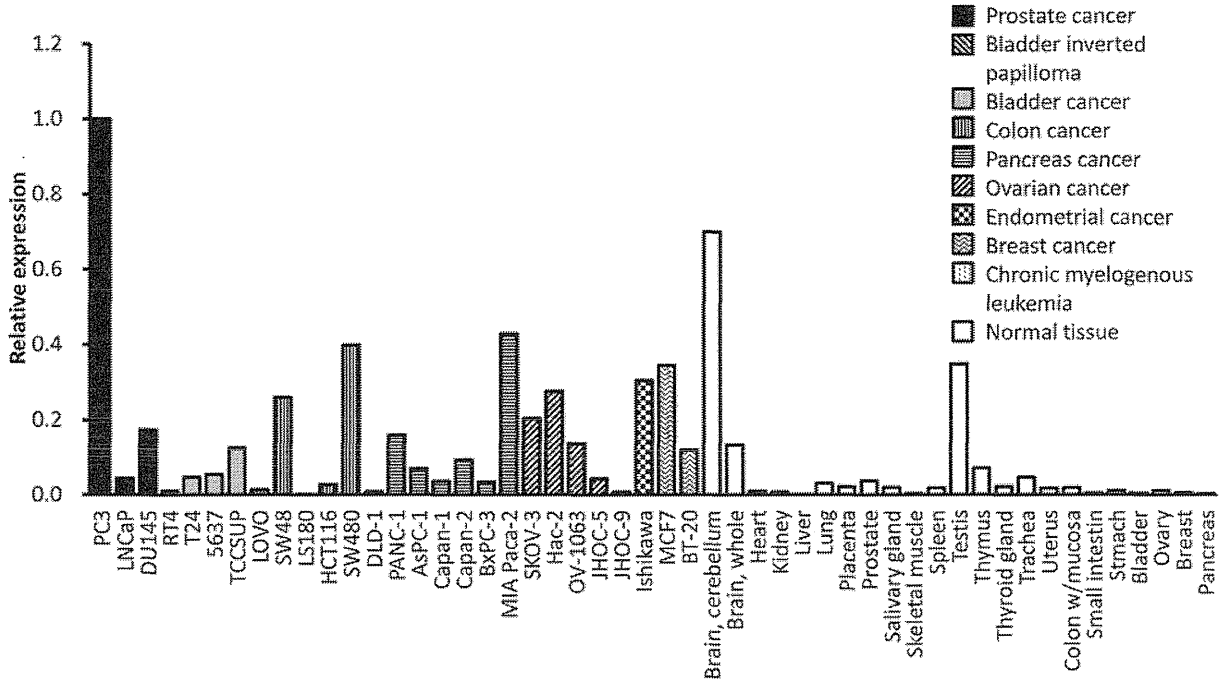

Figure 3. *Expression of C20orf201 mRNA in various cancer cell lines and normal tissues. Expression of mRNA encoding C20orf201 was analyzed by quantitative reverse transcription-polymerase chain reaction and comparative Ct methods. Each mRNA expression was represented as a value to relative PC3 expression. *Not detected.*

antigen family, and, accordingly, peptides obtained by dissociation from HLA molecules might contain a part of antigenic peptide of these cancer-testis antigens. Thus, the structure of 8- or 9-mer peptide containing the identified five or six amino acid sequence might directly indicate the structure for synthetic peptide vaccine which could potentially induce antigen-targeting antitumor immunity. For evaluation of the potential as an immune target recognized by specific CTLs, further studies demonstrating immunogenicity of these peptides in T-cell-mediated antitumor immunity are required.

Identification of novel cancer-associated antigens and determination of the structure of their antigenic peptides have been performed using expression cloning methods or genome-wide exploration with enormous efforts, resulting in generation of many cancer vaccines with low antitumor efficacy. Meanwhile, high-throughput immunoproteomic analysis directly seeking antigenic peptides of cancer associated antigens could provide rapid and efficient generation of effective cancer vaccine because MHC class I peptide actually presented to T-cells are directly collected and analyzed. Immunoproteomic analysis might be also promising in identifying novel biomarkers useful both diagnosis and treatment of cancer.

Acknowledgements

This research was partly supported by The Jikei University Research Fund and KAKENHI (Grant-in-Aid for Young Scientists (B)).

References

1 Mlecnik B, Bindea G, Pagès F and Galon J: Tumor immunosurveillance in human cancers. Cancer Metastasis Rev *30*: 5-12, 2011.

2 Bindea G, Mlecnik B, Fridman WH, Pagès F and Galon J: Natural immunity to cancer in humans. Curr Opin Immunol *22*: 215-222, 2010.

3 Hamaï A, Benlalam H, Meslin F, Hasmim M, Carré T, Akalay I, Janji B, Berchem G, Noman MZ and Chouaib S: Immune surveillance of human cancer: If the cytotoxic T-lymphocytes play the music, does the tumoral system call the tune? Tissue Antigens *75*: 1-8, 2010.

4 Draghiciu O, Nijman HW and Daemen T: From tumor immunosuppression to eradication: Targeting homing and activity of immune effector cells to tumors. Clin Dev Immunol *2011*: 439053, 2011.

5 Stewart TJ and Smyth MJ: Improving cancer immunotherapy by targeting tumor-induced immune suppression. Cancer Metastasis Rev *30*: 125-140, 2011.

6 Bhutia SK, Mallick SK and Maiti TK: Tumour escape mechanisms and their therapeutic implications in combination tumour therapy. Cell Biol Int *34*: 553-563, 2010.

7 Palena C and Schlom J: Vaccines against human carcinomas: Strategies to improve antitumor immune responses. J Biomed Biotechnol *2010*: 380697, 2010.
8 Mocellin S, Pilati P and Nitti D: Peptide-based anticancer vaccines: Recent advances and future perspectives. Curr Med Chem *16*: 4779-4796, 2009.
9 O'Meara MM and Disis ML: Therapeutic cancer vaccines and translating vaccinomics science to the global health clinic: Emerging applications toward proof of concept. OMICS *15*: 579-588, 2011.
10 Adamczyk-Poplawska M, Markowicz S and Jagusztyn-Krynicka EK: Proteomics for development of vaccine. J Proteomics *74*: 2596-2616, 2011.
11 Shetty V, Sinnathamby G, Nickens Z, Shah P, Hafner J, Mariello L, Kamal S, Vlahović G, Lyerly HK, Morse MA and Philip R: MHC class I-presented lung cancer-associated tumor antigens identified by immunoproteomics analysis are targets for cancer-specific T-cell response. J Proteomics *74*: 728-743, 2011.
12 Seliger B, Dressler SP, Massa C, Recktenwald CV, Altenberend F, Bukur J, Marincola FM, Wang E, Stevanovic S and Lichtenfels R: Identification and characterization of human leukocyte antigen class I ligands in renal cell carcinoma cells. Proteomics *11*: 2528-2541, 2011.
13 Morse MA, Secord AA, Blackwell K, Hobeika AC, Sinnathamby G, Osada T, Hafner J, Philip M, Clay TM, Lyerly HK and Philip R: MHC class I-presented tumor antigens identified in ovarian cancer by immunoproteomic analysis are targets for T-cell responses against breast and ovarian cancer. Clin Cancer Res *17*: 3408-3419, 2011.
14 Matharoo-Ball B, Ball G and Rees R: Clinical proteomics: Discovery of cancer biomarkers using mass spectrometry and bioinformatics approaches – a prostate cancer perspective. Vaccine *25(Suppl 2)*: B110-121, 2007.
15 Apetoh L, Obeid M, Tesniere A, Ghiringhelli F, Fimia GM, Piacentini M, Kroemer G and Zitvogel L: Immunogenic chemotherapy: Discovery of a critical protein through proteomic analyses of tumor cells. Cancer Genomics Proteomics *4*: 65-70, 2007.
16 Ramakrishna V, Ross MM, Petersson M, Gatlin CC, Lyons CE, Miller CL, Myers HE, McDaniel M, Karns LR, Kiessling R, Parmiani G and Flyer DC: Naturally occurring peptides associated with HLA-A2 in ovarian cancer cell lines identified by mass spectrometry are targets of HLA-A2-restricted cytotoxic T-cells. Int Immunol *15*: 751-763, 2003.
17 Homma S, Koido S, Sagawa Y, Suzuki H, Komita H, Nagasaki E, Takahara A, Horiguchi-Yamada J, Tajiri H, Zeldin DC and Obata T: Antigenic stimulation with cytochrome P450 2J expressed in mouse hepatocellular carcinoma cells regulates host anti-tumour immunity. Clin Exp Immunol *156*: 344-352, 2009.
18 Honma I, Torigoe T, Hirohashi Y, Kitamura H, Sato E, Masumori N, Tamura Y, Tsukamoto T and Sato N: Aberrant expression and potency as a cancer immunotherapy target of alpha-methylacyl-coenzyme A racemase in prostate cancer. J Transl Med *7*: 103, 2009.
19 Herr W, Ranieri E, Gambotto A, Kierstead LS, Amoscato AA, Gesualdo L and Storkus WJ: Identification of naturally processed and HLA-presented Epstein-Barr virus peptides recognized by CD4(+) or CD8(+) T lymphocytes from human blood. Proc Natl Acad Sci USA *96*: 12033-12038, 1999.
20 Ray ME, Su YA, Meltzer PS and Trent JM: Isolation and characterization of genes associated with chromosome-6 mediated tumor suppression in human malignant melanoma. Oncogene *12*: 2527-2533, 1996.
21 Ray ME, Wistow G, Su YA, Meltzer PS and Trent JM: AIM1, a novel non-lens member of the betagamma-crystallin superfamily, is associated with the control of tumorigenicity in human malignant melanoma. Proc Natl Acad Sci USA *94*: 3229-3234, 1997.
22 Vainio P, Mpindi JP, Kohonen P, Fey V, Mirtti T, Alanen KA, Perälä M, Kallioniemi O and Iljin K: High-throughput transcriptomic and RNAi analysis identifies AIM1, ERGIC1, TMED3 and TPX2 as potential drug targets in prostate cancer. PLoS One *7*: e39801, 2012.
23 Strausberg RL, Feingold EA, Grouse LH, Derge JG, Klausner RD, Collins FS, Wagner L, Shenmen CM, Schuler GD, Altschul SF, Zeeberg B, Buetow KH, Schaefer CF, Bhat NK, Hopkins RF, Jordan H, Moore T, Max SI, Wang J, Hsieh F, Diatchenko L, Marusina K, Farmer AA, Rubin GM, Hong L, Stapleton M, Soares MB, Bonaldo MF, Casavant TL, Scheetz TE, Brownstein MJ, Usdin TB, Toshiyuki S, Carninci P, Prange C, Raha SS, Loquellano NA, Peters GJ, Abramson RD, Mullahy SJ, Bosak SA, McEwan PJ, McKernan KJ, Malek JA, Gunaratne PH, Richards S, Worley KC, Hale S, Garcia AM, Gay LJ, Hulyk SW, Villalon DK, Muzny DM, Sodergren EJ, Lu X, Gibbs RA, Fahey J, Helton E, Ketteman M, Madan A, Rodrigues S, Sanchez A, Whiting M, Madan A, Young AC, Shevchenko Y, Bouffard GG, Blakesley RW, Touchman JW, Green ED, Dickson MC, Rodriguez AC, Grimwood J, Schmutz J, Myers RM, Butterfield YS, Krzywinski MI, Skalska U, Smailus DE, Schnerch A, Schein JE, Jones SJ and Marra MA: Mammalian Gene Collection Program Team. Generation and initial analysis of more than 15,000 full-length human and mouse cDNA sequences. Proc Natl Acad Sci USA *99*: 16899-16903, 2002.
24 Scanlan MJ, Gure AO, Jungbluth AA, Old LJ and Chen YT: Cancer/testis antigens: An expanding family of targets for cancer immunotherapy. Immunol Rev *188*: 22-32, 2002.
25 Lim SH, Zhang Y and Zhang J: Cancer-testis antigens: The current status on antigen regulation and potential clinical use. Am J Blood Res *2*: 29-35, 2012.
26 Caballero OL and Chen YT: Cancer/testis (CT) antigens: Potential targets for immunotherapy. Cancer Sci *100*: 2014-2021, 2009.
27 Cheng YH, Wong EW and Cheng CY: Cancer/testis (CT) antigens, carcinogenesis and spermatogenesis. Spermatogenesis. *1*: 209-220, 2011.
28 Meek DW and Marcar L: MAGE-A antigens as targets in tumour therapy. Cancer Lett *324*: 126-132, 2012.
29 Gnjatic S, Nishikawa H, Jungbluth AA, Güre AO, Ritter G, Jäger E, Knuth A, Chen YT and Old LJ: NY-ESO-1: Review of an immunogenic tumor antigen. Adv Cancer Res *95*: 1-30, 2006.

Received March 14, 2013
Revised April 1, 2013
Accepted April 3, 2013

Journal of Human Genetics (2014) 59, 78–87

www.nature.com/jhg

ORIGINAL ARTICLE

The tumor-suppressive *microRNA-143/145* cluster inhibits cell migration and invasion by targeting *GOLM1* in prostate cancer

Satoko Kojima[1,4], Hideki Enokida[2,4], Hirofumi Yoshino[2], Toshihiko Itesako[2], Takeshi Chiyomaru[2], Takashi Kinoshita[3], Miki Fuse[3], Rika Nishikawa[3], Yusuke Goto[3], Yukio Naya[1], Masayuki Nakagawa[2] and Naohiko Seki[3]

Our recent study of microRNA (miRNA) expression signature of prostate cancer (PCa) has revealed that the *microRNA-143/145* (*miR-143/145*) cluster is significantly downregulated in cancer tissues, suggesting that these cluster miRNAs are candidate tumor suppressors. The aim of this study was to investigate the functional significance of the *miR-143/145* cluster in PCa cells and to identify novel targets regulated by these cluster miRNAs in PCa. Restoration of *miR-143 or miR-145* in PCa cell lines (PC3 and DU145) revealed that these miRNAs significantly inhibited cancer cell migration and invasion. Gene expression data and *in silico* analysis demonstrated that Golgi membrane protein 1 (*GOLM1*) resembling a type II golgi transmembrane protein was a potential target of *miR-143/145* cluster target gene. Gene expression studies and luciferase reporter assays showed that *GOLM1* was directly regulated by the *miR-143/145* cluster. Silencing of *GOLM1* resulted in significant inhibition of cell migration and invasion in PCa cells. Furthermore, the expression of GOLM1 was upregulated in cancer tissues by immunohistochemistry. Loss of the tumor-suppressive *miR-143/145* cluster enhanced cancer cell migration and invasion in PCa through directly regulating *GOLM1*. Our data on target genes regulated by the tumor-suppressive *miR-143/145* cluster provide new insights into the potential mechanisms of PCa oncogenesis and metastasis.
Journal of Human Genetics (2014) **59**, 78–87; doi:10.1038/jhg.2013.121; published online 28 November 2013

Keywords: GOLM1; microRNA; *miR-143*; *miR-145*; prostate cancer; tumor suppressor

INTRODUCTION

Prostate cancer (PCa) is the most frequently diagnosed cancer and the second leading cause of cancer death among men in developed countries.[1] Most patients are initially responsive to androgen-deprivation therapy, but their cancers eventually become resistant to androgen-deprivation therapy and progress to castration-resistant prostate cancer (CRPC). Currently, CRPC is difficult to treat, and most clinical trials for advanced PCa have shown limited benefits, with disease progression and metastasis to the bone or other sites.[2,3] Therefore, understanding the molecular mechanisms of CRPC and metastatic pathways underlying PCa using currently available genomic approaches would help to improve therapies for and prevention of the disease.

The discovery of non-coding RNAs (ncRNAs) in the human genome was an important conceptual breakthrough in the post-genome sequencing era.[4] Improving our understanding of ncRNAs is necessary for continued progress in cancer research. MicroRNAs (miRNAs) are endogenous small ncRNA molecules (19–22 bases in length) that regulate protein-coding gene expression by repressing translation or cleaving RNA transcripts in a sequence-specific manner. Currently, 2042 human mature miRNAs are registered at miRBase release 19.0 (http://microrna.sanger.ac.uk/). miRNAs are unique in their ability to regulate multiple protein-coding genes. Bioinformatic predictions indicate that miRNAs regulate >30–60% of the protein-coding genes in the human genome.[5,6]

Emerging evidence has demonstrated that miRNAs are aberrantly expressed in many human cancers and have significant roles in the initiation, development and metastasis of these cancers.[7,8] It is believed that normal regulatory mechanisms can be disrupted by the aberrant expression of tumor suppressive or oncogenic miRNAs in cancer cells. Therefore, identification of aberrantly expressed miRNAs is the first step toward elucidating miRNA-mediated oncogenic pathways. Based on this, we identified miRNA expression signature in PCa using clinical specimens and found that *miR-145* expression was significantly downregulated in PCa.[9] We also reported that *miR-145* suppresses cell proliferation, migration and invasion by

[1]Department of Urology, Teikyo University Chiba Medical Center, Chiba, Japan; [2]Department of Urology, Graduate School of Medical and Dental Sciences, Kagoshima University, Kagoshima, Japan and [3]Department of Functional Genomics, Graduate School of Medicine, Chiba University, Chiba, Japan
[4]These authors contributed equally to this work.
Correspondence: Dr N Seki, Department of Functional Genomics, Graduate School of Medicine, Chiba University, 1-8-1 Inohana Chuo-ku, Chiba 260 8670, Japan.
E-mail: naoseki@faculty.chiba-u.jp
Received 21 September 2013; revised 28 October 2013; accepted 28 October 2013; published online 28 November 2013

targeting *FSCN1*.[10,11] Other studies have reported that the *miR-143/145* cluster is significantly downregulated in PCa and have suggested its important association with oncogenesis and bone metastasis in PCa.[12,13]

The aim of the present study was to investigate the functional significance of the *miR-143/145* cluster and to identify the molecular targets regulated by this cluster in PCa cells. Genome-wide gene expression data and *in silico* database analysis showed that Golgi membrane protein 1 (*GOLM1*) was a promising candidate target of the *miR-143/145* cluster. GOLM1, also known as Golgi phosphoprotein 2 (*GOLPH2*) and Golgi protein 73 (*GP73*), is a newly identified Golgi-associated protein. Although the functional roles of GOLM1 are currently unclear, GOLM1 has been shown to interact with other proteins through its transmembrane protein domain.[14] The overexpression of GOLM1 has been reported in several types of cancers, including PCa.[15–17] Elucidation of the molecular targets regulated by the tumor-suppressive *miR-143/145* cluster will provide new insights into the potential molecular mechanisms of PCa oncogenesis and metastasis and will facilitate the development of novel therapeutic strategies for the treatment of PCa.

MATERIALS AND METHODS

Clinical prostate specimens

Clinical specimens were obtained from patients at the Teikyo University Chiba Medical Center from 2008 to 2013. All the patients had elevated levels of prostate-specific antigen and had undergone transrectal prostate needle biopsy. Non-cancerous prostate tissue ($n=24$) was obtained from patients who were negative for malignancy without indurations on the prostate. Prostate tumor tissues ($n=28$) contained 90–100% malignant cells in the biopsy cores. Patients' characteristics are shown in Table 1. Before tissue collection, all patients provided written informed consent of tissue donation for research purposes. The protocol was approved by the Institutional Review Board of Teikyo University.

Cell culture

PC3 and DU145 cells, human PCa cells obtained from the American Type Culture Collection (Manassas, VA, USA), were maintained in RPMI-1640 medium supplemented with 10% fetal bovine serum in a humidified atmosphere of 5% CO_2 and 95% air at 37 °C.

RNA extraction

Total RNA was isolated using TRIzol reagent (Invitrogen, Carlsbad, CA, USA) according to the manufacturer's protocol. RNA concentrations were determined spectrophotometrically, and molecular integrity was checked by gel electrophoresis. RNA quality was confirmed using an Agilent 2100 Bioanalyzer (Agilent Technologies, Santa Clara, CA, USA).

Quantitative real-time reverse transcriptase–PCR (RT-PCR)

First-strand cDNA was synthesized from 1 μg total RNA using a High Capacity cDNA Reverse Transcription Kit (Applied Biosystems, Foster City, CA, USA). Gene-specific PCR products were assayed continuously using a 7900-HT Real-Time PCR System (Applied Biosystems) according to the manufacturer's protocol. The initial PCR step consisted of a 10-min hold at 95 °C, followed by 40 cycles consisting of a 15-s denaturation at 95 °C and a 1-min annealing/extension at 63 °C. TaqMan probes and primers for *GOLM1* (P/N: Hs00213061_m1) and *GAPDH* (P/N: Hs02758991_g1) as an internal control were obtained from Applied Biosystems (Assay-On-Demand Gene Expression Products). The expression levels of *miR-143* (Assay ID: 002249) and *miR-145* (Assay ID: 002278) were analyzed by TaqMan quantitative real-time PCR (TaqMan MicroRNA Assay; Applied Biosystems) and normalized to the expression of *RNU48* (Assay ID: 001006). The delta delta Ct method was used to calculate the relative quantities of target genes. All reactions were performed in triplicate, and each assay included negative control reactions that lacked cDNA.

Transfections with mature miRNA and small interfering RNA (siRNA)

The following mature miRNA species were used in this study: Pre-miR miRNA Precursor for hsa-miR-143 (Product ID: PM10883) and hsa-miR-145 (Product ID: PM11480; Applied Biosystems). The following siRNAs were used: Stealth Select RNAi siRNA, si-GOLM1 (Cat no. HSS181966 and HSS181968; Invitrogen), and negative control miRNA/siRNA (P/N: AM17111; Applied Biosystems). RNAs were incubated with OPTI-MEM (Invitrogen) and Lipofectamine RNAiMax reagent (Invitrogen) as described previously. The transfection efficiency of miRNA in PC3 and DU145 cells was confirmed based on downregulation of *TWF1* (*PTK9*) mRNA following transfection with *miR-1* as previously reported.

Cell proliferation, migration and invasion assays

Cells were transfected with 10 nM miRNA or siRNA by reverse transfection and plated in 96-well plates at 3×10^3 cells per well. After 72 h, cell proliferation was determined with the XTT assay using a Cell Proliferation Kit II (Roche Molecular Biochemicals, Mannheim, Germany) as previously reported.[18,19]

Cell migration was evaluated with a wound-healing assay. Cells were plated in six-well plates, and the cell monolayers were scraped using a P-20 micropipette tip. The initial gap length (0 h) and the residual gap length at 24 h after wounding were calculated from photomicrographs.

A cell invasion assay was carried out using modified Boyden chambers containing Transwell-precoated Matrigel membrane filter inserts with 8-μm pores in 24-well tissue culture plates (BD Biosciences, Bedford, MA, USA) at 2×10^5 cells per well. Cells were transfected with 10 nM miRNA or siRNA by reverse transfection and plated in 10-cm dishes at 8×10^5 cells per dish. After 48 h, the cells were collected, and 2×10^5 cells were added to the upper chamber of each migration well. Cells were allowed to invade for 48 h. After gentle removal of the non-migratory cells from the filter surface of the upper chamber, the cells that invaded into the lower chamber were fixed and stained with Diff-Quick (Sysmex Corporation, Kobe, Japan). The number of cells that migrated to the lower surface was determined microscopically by counting four areas of constant size per well.

All experiments were performed in triplicate.

Western blotting

Cells were harvested 72 h after transfection, and lysates were prepared. Fifty micrograms of protein lysate was separated on Mini-PROTEAN TGX gels (Bio-Rad, Hercules, CA, USA) and transferred to polyvinylidene difluoride membranes. Immunoblotting was performed with rabbit anti-GOLM1 antibodies (1:500; HPA010638, Sigma-Aldrich, St Louis, MO, USA) and anti-GAPDH antibodies (1:1000; ab8245, Abcam, Cambridge, UK), used as an internal loading control. Membranes were washed and incubated with anti-mouse immunoglobulin G horseradish peroxidase-linked antibodies (No. 7076, Cell Signaling Technology, Danvers, MA, USA). Complexes were visualized with an Immun-Star WesternC Chemiluminescence Kit (Bio-Rad), and the expression levels of these genes were evaluated by the ImageJ software provided by National Institutes of Health (NIH), Bethesda, MD, USA (ver.1.44; http://rsbweb.nih.gov/ij/).

Genome-wide gene expression and *in silico* analyses for the identification of genes regulated by the *miR-143/145* cluster

To gain further insight into which genes were affected by the *miR-143/145* cluster, we performed a combination of *in silico* and genome-wide gene expression analyses. First, genes regulated by the *miR-143/145* cluster were listed using the TargetScan database as described previously.[18,19] To investigate the expression status of candidate of *miR-143/145* cluster-target genes in PCa clinical specimens, we examined the gene expression profiles in the GEO database (accession number: GSE29079). In this expression study, tissue samples from 47 PCa with clinical high-risk tumors were included, and none of the patients had been treated with neo-adjuvant treatments, such as radiation, cytotoxic and endocrine therapies.[20]

To identify molecular pathways regulated by *miR-143/145* cluster in PCa, upregulated genes which were targeted by *miR-143/145* cluster were analyzed in terms of Kyoto Encyclopedia of Genes and Genomes (KEGG) pathway categories using the GENECODIS program (http://genecodis.cnb.csic.es/).

Table 1 Patient characteristics

No.	*pCa or non-Pca*	*Age*	*PSA (ng ml^{-1})*	*Gleason Score*	*Stage*	*TNM classification*		
						T	*N*	*M*
1	Pca	67	244	4+4	D2	4	1	1
2	Pca	70	395	4+4	D2	3a	1	1
3	Pca	83	49.9	4+5	C	3a	0	0
4	Pca	68	212	4+4	D1	3b	1	0
5	Pca	80	589	4+5	D1	3b	1	0
6	Pca	72	2530	4+5	D2	3a	1	1
7	Pca	76	12.5	4+5	D2	3b	1	1
8	Pca	67	153	4+4	D2	4	1	1
9	Pca	82	809	4+5	D2	4	1	1
10	Pca	88	50.5	4+4	C	3a	0	0
11	Pca	69	3.5	4+3	C	3a	0	0
12	Pca	64	486	4+5	D2	4	1	1
13	Pca	74	60.8	5+5	D2	4	1	1
14	Pca	63	49.6	4+4	D1	3b	1	0
15	Pca	69	1060	4+5	D2	4	1	1
16	Pca	79	3750	4+4	D2	3a	0	1
17	Pca	78	1400	4+4	D2	3a	0	1
18	Pca	77	2640	4+4	D2	4	1	1
19	Pca	65	82.3	4+4	D2	4	1	1
20	Pca	69	554	4+4	D2	3b	1	1
21	Pca	70	1030	4+4	D2	3b	1	1
22	Pca	78	892	4+5	D2	4	1	1
23	Pca	67	64.6	4+5	D2	3b	0	1
24	Pca	67	34.9	4+4	D2	3b	1	1
25	Pca	64	7.2	4+4	D1	3b	1	0
26	Pca	82	59.5	4+5	C	3b	0	0
27	Pca	86	24.2	4+4	C	3b	0	0
28	Pca	71	63.8	4+3	C	3a	0	0
1	Non-Pca	69	12.2	—	—	—	—	—
2	Non-Pca	66	11.9	—	—	—	—	—
3	Non-Pca	85	10.1	—	—	—	—	—
4	Non-Pca	55	11.2	—	—	—	—	—
5	Non-Pca	58	5.9	—	—	—	—	—
6	Non-Pca	67	22.0	—	—	—	—	—
7	Non-Pca	67	7.3	—	—	—	—	—
8	Non-Pca	69	7.9	—	—	—	—	—
9	Non-Pca	68	7.2	—	—	—	—	—
10	Non-Pca	53	4.3	—	—	—	—	—
11	Non-Pca	62	5.1	—	—	—	—	—
12	Non-Pca	63	10.0	—	—	—	—	—
13	Non-Pca	62	5.1	—	—	—	—	—
14	Non-Pca	74	8.3	—	—	—	—	—
15	Non-Pca	65	4.3	—	—	—	—	—
16	Non-Pca	72	5.4	—	—	—	—	—
17	Non-Pca	66	5.4	—	—	—	—	—
18	Non-Pca	67	5.0	—	—	—	—	—
19	Non-Pca	66	19.5	—	—	—	—	—
20	Non-Pca	53	6.7	—	—	—	—	—
21	Non-Pca	63	5.3	—	—	—	—	—
22	Non-Pca	66	7.7	—	—	—	—	—
23	Non-Pca	57	7.3	—	—	—	—	—
24	Non-Pca	63	12.9	—	—	—	—	—

Abbreviations: PCa, prostate cancer; PSA, prostate-specific antigen; TNM, Tumor, Node, Metastatis.

Plasmid construction and dual-luciferase reporter assay

Partial wild-type sequences of the *GOLM1* 3′ untranslated region (UTR) or those with a deleted *miR-143* target site (position 1610–1617 of the *GOLM1* 3′UTR) and deleted *miR-145* target sites (positions 5–12 and 260–267 of the *GOLM1* 3′UTR) were inserted between the XhoI–PmeI restriction sites in the 3′UTR of the *hRluc* gene in the psiCHECK-2 vector (C8021; Promega,

Madison, WI, USA). The protocol for vector construction was described previously.[18,19] Sequences of the oligonucleotides are described in Supplementary Table S1. The synthesized DNA was cloned into the psiCHECK-2 vector. PC3 cells were transfected with 50 ng of the vector and 10 nM *miR-143* or *miR-145* using Lipofectamine 2000 (Invitrogen). The activities of firefly and renilla luciferases in cell lysates were determined with a dual-luciferase assay system (E1910; Promega). Normalized data were calculated as the ratio of renilla/firefly luciferase activities.

Immunohistochemistry

A tissue microarray of 39 prostate tumors and 8 normal prostate tissues was obtained from US Biomax, Inc. (PR956; Rockville, MD, USA). Detailed information on all tumor specimens can be found at http://www.biomax.us/index.php. The patients' backgrounds and clinicopathological characteristics are summarized in Supplementary Table S2. The tissue microarray was immunostained with an UltraVision Detection System (Thermo Scientific) following the manufacturer's protocol. Primary rabbit polyclonal antibodies against GOLM1 (Sigma-Aldrich) were diluted 1:500. The slides were treated with biotinylated goat antibodies. Diaminobenzidine hydrogen peroxidase was the chromogen, and counterstaining was performed with 0.5% hematoxylin. Immunostaining was evaluated according to a scoring method described previously.[18,21] Each case was scored on the basis of the intensity and area of staining. The intensity of staining was graded on the following scale: 0, no staining; 1+, mild staining; 2+, moderate staining; and 3+, intense staining. The area of staining was evaluated as follows: 0, no staining of cells in any microscopic fields; 1+, <30% of cells stained positive; 2+, 30–60% of cells stained positive; 3+, >60% of cells stained positive. A combined staining score (intensity + extension) of <2 indicated low expression, a score between 3 and 4 indicated moderate expression, and a score between 5 and 6 indicated high expression.

Statistical analysis

The relationships between two groups and the numerical values obtained by real-time RT-PCR were analyzed using the paired *t*-test. The relationship among three variables and numerical values was analyzed using the Bonferroni-adjusted Mann–Whitney *U* test. All analyses were performed using Expert StatView software (version 4, SAS Institute Inc., Cary, NC, USA).

RESULTS

The expression levels of *miR-143* and *miR-145* in PCa specimens

We evaluated the expression levels of *miR-143* and *miR-145* in normal prostate tissues ($n=24$) and PCa tissues ($n=28$). Prostate-specific antigen levels in patients with normal prostate tissues were measured to have a median value of 8.7 ng ml^{-1} (range 4.3–22 ng ml^{-1}), whereas PCa patients had high prostate-specific antigen values, with a median of 182 ng ml^{-1} (3.4–3750 ng ml^{-1}). PCa patients had progressive disease with N1 (67.8%) and M1 (64.2%) according to TNM (Tumor, Node, Metastatis) classification (Table 1).

The expression levels of *miR-143* and *miR-145* were determined by RT-PCR. The expression levels of *miR-143* (Figure 1a) and *miR-145* (Figure 1b) were significantly lower in PCa tissues compared with normal tissues ($P=0.00148$ and $P<0.0001$, respectively). The expression of *miR-143* was highly correlated with that of *miR-145* (correlation coefficient, 0.898; $P<0.0001$; Figure 1c).

Effects of *miR-143* and *miR-145* transfection on cell proliferation, migration and invasion in PCa cells

Next, the expression levels of *miR-143* and *miR-145* in DU145 and PC3 cells were determined by RT-PCR and were compared with those of normal prostate tissues. *miR-143* and *miR-145* were significantly downregulated in DU145 and PC3 cells as compared with normal prostates (Figures 1a and b).

To examine the functional roles of *miR-143* and *miR-145*, we performed gain-of-function studies using miRNA transfection into DU145 and PC3 cells. XTT assays revealed significant inhibition of cell proliferation in DU145 and PC3 cells transfected with *miR-143* and *miR-145* in comparison with mock-transfected cells and control transfectants (cell proliferation, percentage of mock: DU145 cells 68.8% ± 3.7%, 53.4% ± 1.1%, 100.0% ± 1.3% and 93.7% ± 1.7%, respectively, $P<0.0001$; PC3 cells 90.4% ± 5.7%, 60.0% ± 1.2%, 100.0% ± 3.3% and 103.2% ± 4.0%, respectively, $P=0.0969$ and $P<0.0005$; Figure 2a).

Moreover, wound-healing assays demonstrated significant inhibition of cell migration in DU145 and PC3 cells transfected with *miR-143* and *miR-145* in comparison with mock-transfected cells and control transfectants (cell migration, percentage of mock: DU145 cells 64.2% ± 5.2%, 59.0% ± 10.0%, 100.0% ± 7.1% and 88.7% ± 8.8%, respectively, $P=0.0047$ and $P=0.0016$; PC3 cells 68.9% ± 4.5%, 10.7% ± 4.9%, 100.0% ± 5.8% and 103.6% ± 7.7%, respectively, $P=0.0013$ and $P<0.0001$; Figure 2b).

Similarly, Matrigel invasion assays revealed that transfection with these miRNAs reduced cell invasion. Indeed, the number of invading cells was significantly decreased in DU145 and PC3 cells transfected with *miR-143* and *miR-145* in comparison with mock-transfected cells and control transfectants (percentage of invading cells: DU145 cells 59.7% ± 7.3%, 12.1% ± 2.8%, 100.0% ± 4.9% and 114.1% ± 3.3%, respectively, $P<0.0001$; PC3 cells 90.8% ± 3.2%, 17.7% ± 1.9%, 100.0% ± 6.7% and 103.6% ± 4.2%, respectively, $P=0.1539$ and $P<0.0001$; Figure 2c).

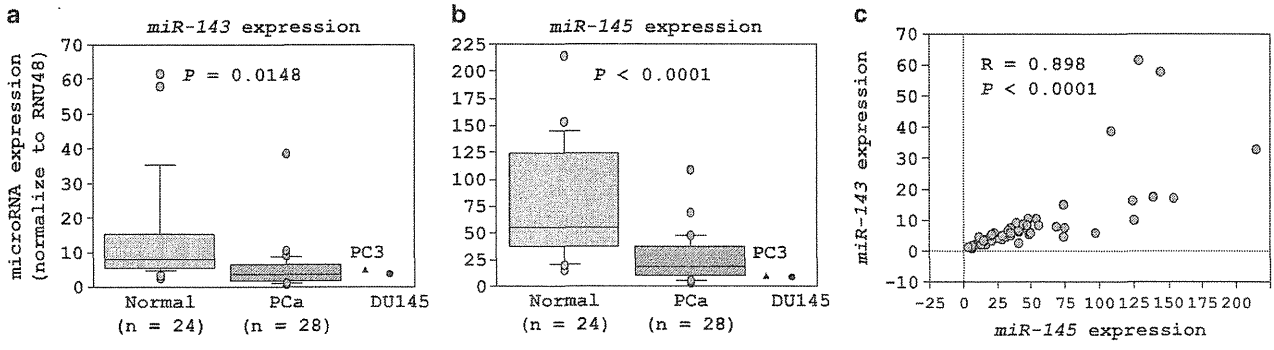

Figure 1 Expression levels of *miR-143* and *miR-145*. (**a**, **b**) *miR-143* and *miR-145* expression levels in clinical PCa specimens and PCa cell lines (PC3 and DU145) compared with non-cancerous tissues. *RNU48* was used as the internal control. (**c**) Correlation between the relative expression level of *miR-143* (*x*-axis) and that of *miR-145* (*y*-axis). Levels are plotted as a scatterplot.

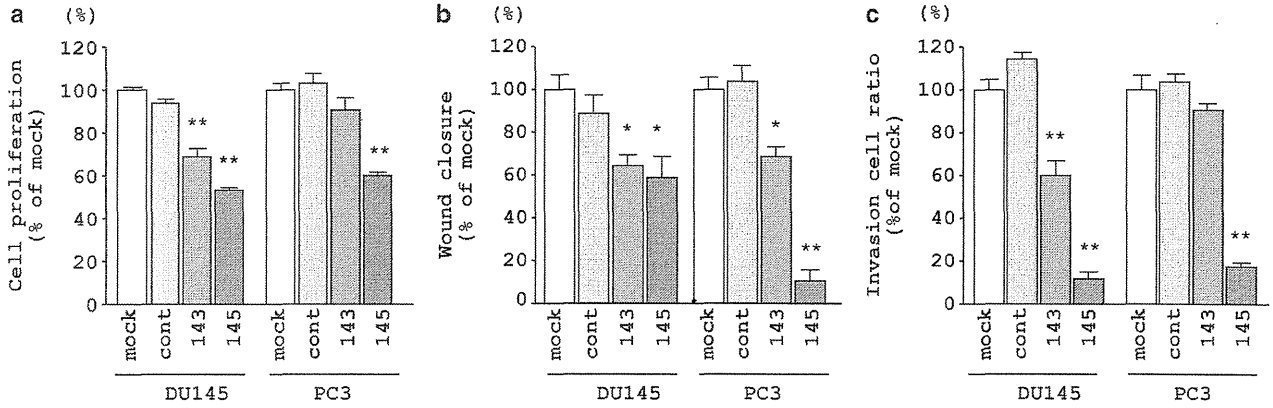

Figure 2 Effects of transfection with mature *miR-143* and *miR-145* on RCC cell lines. (a) Cell proliferation was determined with XTT assays in PC3 and DU145 cell lines after 72 h of transfection with 10 nM *miR-143*, *miR-145*, miR-control or mock transfection. (b) Cell migration activity was determined by the wound-healing assay. (c) Cell invasion activity was determined by Matrigel invasion assay. $^{*}P<0.01$; $^{**}P<0.0001$.

Identification of targets genes regulated by the *miR-143/145* cluster in PCa

To gain further insight into the molecular mechanisms and pathways regulated by the tumor-suppressive *miR-143/145* cluster in PCa, we performed a combination of gene expression and *in silico* analyses. The strategy of selection of *miR-143/145* cluster-regulated genes is shown in Figure 3. The TargetScan program showed that 1053 genes had putative target sites for both *miR-143* and *miR-145* in their 3′UTR regions. To confirm the expression levels of these genes in clinical prostate tissues, GEO database (GEO accession number: GSE29079) analysis was performed. Among the 1053 genes, 347 genes were upregulated in 47 PCa specimens compared with 48 non-cancerous prostate tissues. Expression data for the 44 genes (>1.5 fold change) are summarized in Table 2, and the other upregulated genes are shown in Supplementary Table S2.

Furthermore, those 347 genes were classified KEGG pathways using GeneCodis program to identify molecular pathways regulated by *miR-143/145* cluster in PCa. Four signaling pathways (endocytosis, oocyte meiosis, protein processing in endoplasmic reticulum and ubiquitin-mediated proteolysis) were identified in this analysis (Supplementary Tables S3A–E).

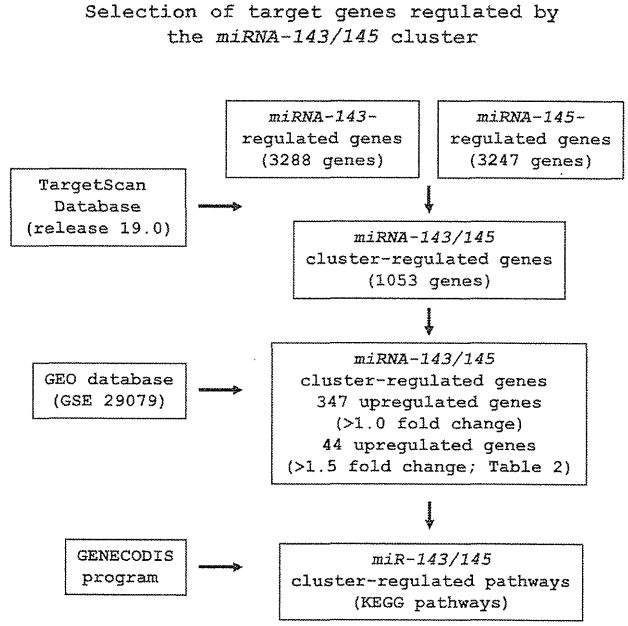

Figure 3 Flow chart of the strategy for analysis of *miR-143/145* cluster target genes. A total of 1053 genes were selected as putative *miR-143/145* cluster target genes by TargetScan database analysis. We then analyzed the expression levels of these 1053 genes by using available data sets of GEO (GSE 29079). The analyses showed that 44 genes were significantly upregulated in PCa specimens compared with normal specimens.

GOLM1 as a target of post-transcriptional repression by the *miR-143/145* cluster in PCa cells

The mRNA and protein expression levels of GOLM1 were markedly downregulated in *miR-143*- and *miR-145*-transfected PC3 and DU145 cells in comparison with mock-transfected cells and control transfectants (Figures 4a and b). Therefore, we next performed a luciferase reporter assay to determine whether *GOLM1* mRNA had functional target sites for *miR-143* and *miR-145*. We used three vectors encoding the partial sequences of the 3′UTR of *GOLM1* mRNA (Figure 4c, Supplementary Table S1). The luminescence intensity was significantly decreased in the presence of two sites targeted by *miR-143* or *miR-145* (positions 1610–1617 and 5–12, respectively; Figure 4c, middle and lower panels). In contrast, the luminescence intensity was not decreased by transfection with *miR-145* at position 260–267 or with deleted sequences of either miRNA (Figure 4c, middle panel). These data suggested that *miR-143* and *miR-145* bound directly to specific sites in the 3′UTR of *GOLM1* mRNA.

Effects of *GOLM1* knockdown on cell proliferation, migration and invasion in PCa cell lines

The expression of *GOLM1* mRNA was upregulated in DU145 and PC3 cells compared with normal prostate tissues (data not shown). Therefore, to examine the functional role of GOLM1 in PCa, we performed loss-of-function studies using transfection with two different siRNA sequences targeting GOLM1 in DU145 and PC3 cells. The expression of GOLM1 mRNA and protein was markedly repressed in si-GOLM1 transfectants (Figures 5a and b).

XTT assays revealed that transfection with si-GOLM1 inhibited cell proliferation in PC3 cells compared with mock-transfected cells and si-control transfectants; however, no significant inhibition was

Table 2 Identification of target genes regulated by the miR-143/145 cluster in PCa

Entrez gene ID	*Gene symbol*	*Fold change*	*Description*
51280	GOLM1	3.52	Golgi membrane protein 1
28996	HIPK2	2.35	Homeodomain-interacting protein kinase 2
54848	ARHGEF38	2.26	Rho guanine nucleotide exchange factor (GEF) 38
4646	MYO6	2.17	Myosin VI
56894	AGPAT3	2.02	1-Acylglycerol-3-phosphate O-acyltransferase 3
3069	HDLBP	1.95	High-density lipoprotein-binding protein
51114	ZDHHC9	1.92	Zinc finger, DHHC-type containing 9
7764	ZNF217	1.90	Zinc finger protein 217
7941	PLA2G7	1.90	Phospholipase A2, group VII
19	ABCA1	1.80	ATP-binding cassette, sub-family A (ABC1), member 1
11057	ABHD2	1.80	Abhydrolase domain containing 2
27075	TSPAN13	1.79	Tetraspanin 13
22848	AAK1	1.79	AP2-associated kinase 1
51313	FAM198B	1.78	Family with sequence similarity 198, member B
23200	ATP11B	1.78	ATPase, class VI, type 11B
2065	ERBB3	1.72	V-erb-b2 avian erythroblastic leukemia viral oncogene homolog 3
206358	SLC36A1	1.72	Solute carrier family 36 (proton/amino acid symporter), member 1
84914	ZNF587	1.71	Zinc finger protein 587
79939	SLC35E1	1.70	Solute carrier family 35, member E1
3480	IGF1R	1.69	Insulin-like growth factor 1 receptor
2335	FN1	1.68	Fibronectin 1
117177	RAB3IP	1.66	RAB3A-interacting protein
23362	PSD3	1.65	Pleckstrin and Sec7 domain containing 3
57182	ANKRD50	1.64	Ankyrin repeat domain 50
1729	DIAPH1	1.64	Diaphanous-related formin 1
9517	SPTLC2	1.63	Serine palmitoyltransferase, long chain base subunit 2
26999	CYFIP2	1.63	Cytoplasmic FMR1-interacting protein 2
3340	NDST1	1.62	N-deacetylase/N-sulfotransferase (heparan glucosaminyl) 1
9931	HELZ	1.60	Helicase with zinc finger
22834	ZNF652	1.58	Zinc finger protein 652
3488	IGFBP5	1.56	Insulin-like growth factor binding protein 5
27102	EIF2AK1	1.55	Eukaryotic translation initiation factor 2-alpha kinase 1
8243	SMC1A	1.55	Structural maintenance of chromosomes 1A
7311	UBA52	1.55	Ubiquitin A-52 residue ribosomal protein fusion product 1
1601	DAB2	1.53	Dab, mitogen-responsive phosphoprotein, homolog 2 (Drosophila)
11060	WWP2	1.53	WW domain containing E3 ubiquitin protein ligase 2
26472	PPP1R14B	1.52	Protein phosphatase 1, regulatory (inhibitor) subunit 14B
54765	TRIM44	1.52	Tripartite motif containing 44
57493	HEG1	1.52	Heart development protein with EGF-like domains 1
2035	EPB41	1.51	Erythrocyte membrane protein band 4.1 (elliptocytosis 1, RH-linked)
79822	ARHGAP28	1.51	Rho GTPase activating protein 28
2806	GOT2	1.51	Glutamic-oxaloacetic transaminase 2, mitochondrial
6801	STRN	1.51	Striatin, calmodulin-binding protein
57619	SHROOM3	1.51	Shroom family member 3

Abbreviation: PCa, prostate cancer.

observed in DU145 cells (cell proliferation, percentage of mock: DU145 cells 89.5% ± 2.3%, 92.7% ± 2.9%, 100.0% ± 1.9% and 98.5% ± 1.7%, respectively, $P = 0.0033$ and $P = 0.031$; PC3 cells 78.0% ± 1.2%, 81.5% ± 0.9%, 100.0% ± 1.3% and 92.0% ± 1.4%, respectively, $P < 0.0001$, Figure 6a).

Wound-healing assays demonstrated that transfection with the two siRNAs targeting GOLM1 significantly inhibited cell migration compared with mock-transfected cells and control transfectants in PC3 and DU145 cells (cell migration, percentage of mock: DU145 cells 68.5% ± 7.3%, 43.4% ± 4.6%, 100.0% ± 17.7% and 115.6% ± 4.5%, respectively, $P = 0.0389$ and $P = 0.0008$; PC3 cells 39.9% ± 4.7%, 27.8% ± 4.7%, 100.0% ± 2.1% and 105.1% ± 8.2%, respectively, $P < 0.0001$; Figure 6b).

Similarly, Matrigel invasion assays demonstrated that the number of invading cells was significantly decreased si-GOLM1-1 and si-GOLM1-2 transfectants compared with mock-transfected cells and control transfectants, especially in PC3 cells (percentage of invading cells: DU145 cells 70.5% ± 5.4%, 80.9% ± 5.5%, 100.0% ± 4.4% and 127.1% ± 7.0%, respectively, $P = 0.0022$ and $P = 0.0399$; PC3 cells 39.7% ± 2.6%, 8.8% ± 1.0%, 100.0% ± 14.8% and 67.6% ± 9.2%, respectively, $P < 0.0001$; Figure 6c).

Immunohistochemistry for detection of GOLM1 in a PCa tissue microarray

Next, we determined the expression levels of GOLM1 in PCa tissues and normal prostate tissues by immunohistochemical staining.

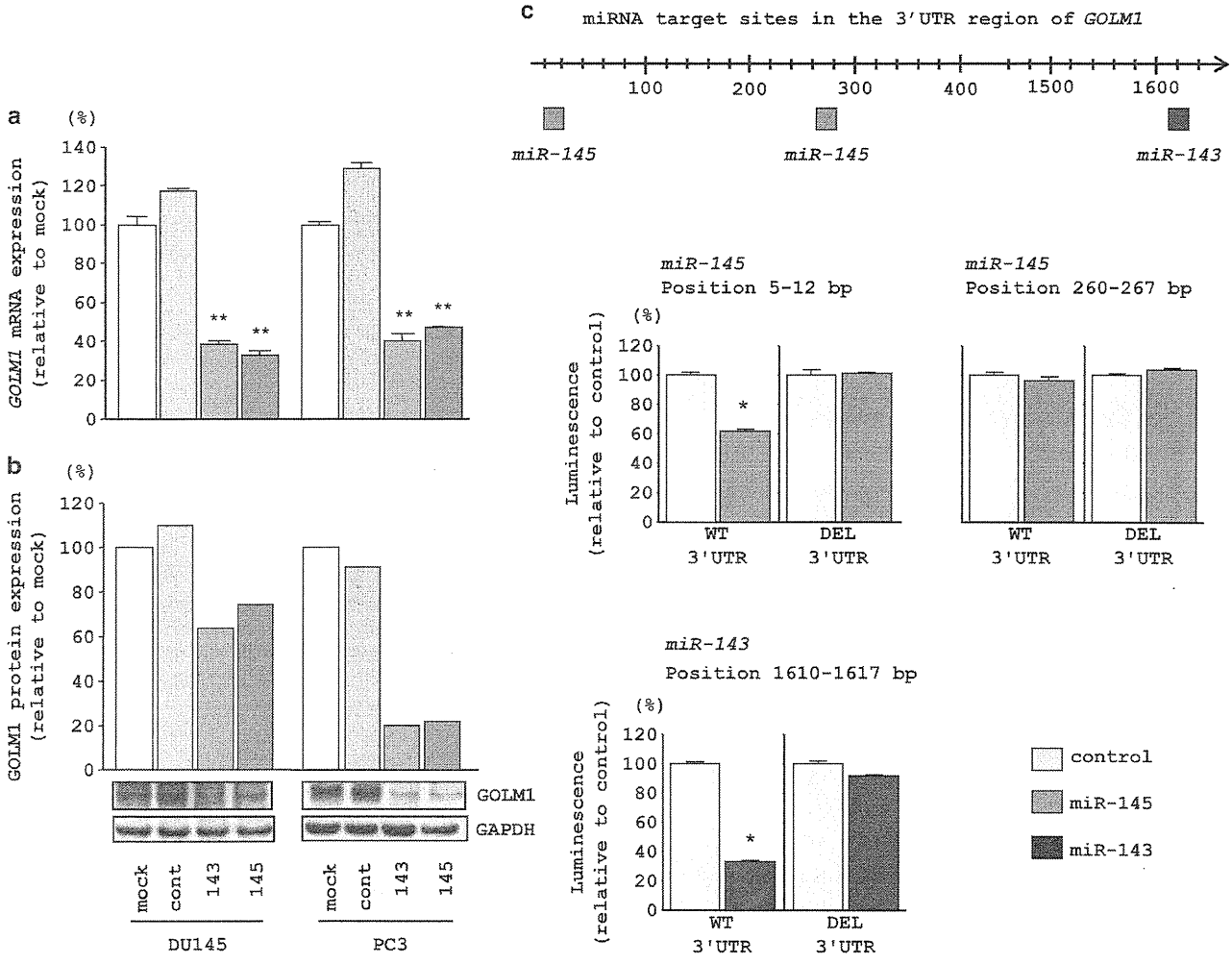

Figure 4 GOLM1 expression was suppressed by *miR-143* and *miR-145* transfection at both the mRNA and protein levels in DU145 and PC3 cells. (**a**) *GOLM1* mRNA expression 72 h after transfection with *miR-143* and *miR-145*. *GAPDH* expression was used for normalization. $^{**}P<0.0001$. (**b**) GOLM1 protein expression 72 h after transfection with *miR-143* and *miR-145*. GAPDH was used as a loading control. (**c**) *miR-143* and *miR-145* binding sites in the 3′UTR of *GOLM1* mRNA. Luciferase reporter assay using the three vectors encoding putative *miR-145* target sites at positions 5–12 and 260–267 and the putative *miR-143* target site at position 1610–1617 for both wild type (WT) and deletion (DEL). Renilla luciferase values were normalized to firefly luciferase values. $^{*}P<0.01$.

GOLM1 was strongly expressed in several tumor lesions (Figures 7a and b), whereas no or low expression was observed in normal tissues (Figure 7c). Moreover, the expression score for GOLM1 protein was significantly higher in PCa tissues than in normal tissues ($P=0.0244$, Figure 7d). The patients' backgrounds and clinicopathological characteristics are summarized in Supplementary Table S4. There were no significant correlations between in GOLM1 expression and the tested clinicopathological parameters (Gleason Score and stages, data not shown).

DISCUSSION

Recent studies of our miRNA expression signatures, including PCa, demonstrated that *miR-143/145* cluster was frequently reduced in cancer tissues.[9,10,18,19] Therefore, it is suggested that the *miR-143/145* cluster have an important tumor-suppressive function in human cancers. In this study, we first tested the expression levels of *miR-143* and *miR-145* in needle biopsy core tissues collected from patients with PCa and non-PCa. We confirmed the reduced expression of both miRNAs in PCa, and expression analysis showed positive correlations between *miR-143* and *miR-145*. These data suggested that *miR-143* and *miR-145* are regulated by the same regulatory systems, and silencing of this miRNA cluster may be a key step in the oncogenesis and progression of PCa. Moreover, *miR-143* and *miR-145* were reported to inhibit stem cell characteristics of PC3 cells, resulting in the inhibition of bone invasion and tumorigenicity of PC3 cells *in vivo*.[12] Others have reported that wild-type p53 suppresses the epithelial–mesenchymal transition and stemness of PC3 cells by modulating *miR-145*.[13] Tumor-suppressor p53 has been reported to transcriptionally regulate *miR-145*, inducing its expression by interaction with a potential p53 response element at the *miR-145* promoter.[22] Interestingly, c-MYC is directly repressed by *miR-145*. These studies indicate that tumor-suppressive *miR-145*, as a new member of the p53 regulatory network, contributes to the direct linkage between p53 and c-MYC in human cancer pathways.[23] Recent studies have shown that the *miR-143/145* cluster is repressed by RAS responsive element-binding protein (RREB1) downstream of

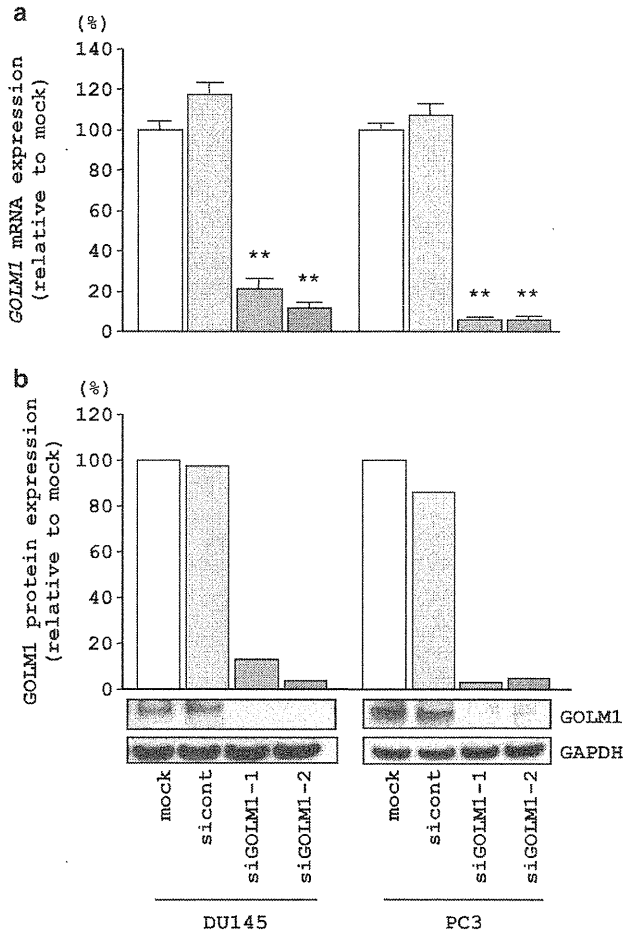

Figure 5 GOLM1 mRNA and protein expression levels were suppressed by si-GOLM1 transfection in DU145 and PC3 cells. (**a**) *GOLM1* mRNA expression 72 h after transfection with si-GOLM1. *GAPDH* expression was used for normalization. $^{**}P<0.0001$. (**b**) GOLM1 protein expression 72 h after transfection with si-GOLM1. GAPDH was used as a loading control. The ratio of GOLM1/GAPDH expression was evaluated using ImageJ software (ver. 1.43; http://rsbweb.nih.gov/ij/index.html).

constitutively active KRAS.[24] Thus, investigation of molecular targets and cancer pathways regulated by the *miR-143/145* cluster is necessary for the clinical development of novel cancer therapeutics.

Researchers are interested in investigating the functional significance of the *miR-143/145* cluster in cancer cells and identifying novel targets commonly regulated by these clustered miRNAs in human cancers, including PCa. Multiple reports have shown that *miR-143* and *miR-145* function as tumor suppressors, targeting a variety of oncogenic genes in several types of cancers.[25,26] Our recent data demonstrated that *miR-143/145* cluster inhibited cancer cell migration and invasion in renal cell carcinoma cells via targeting hexokinase-2, suggesting that this cluster acts as a tumor suppressor in renal cell carcinoma.[27] In this study, we also showed that *miR-143/145* cluster function as a tumor suppressor in PCa. Therefore, identification of *miR-143/145* cluster-regulated cancer pathways may provide new insights into the molecular mechanisms of human cancers.

We hypothesize that identification of novel cancer pathways and target genes regulated by tumor-suppressive miRNAs is an important first step in understanding human oncogenesis. Based on this view, we performed a combination study of genome-wide gene expression analysis in cells transfected with tumor-suppressive miRNAs, *in silico* analysis and identification of novel miRNA-regulated cancer pathways and targets, as reported previously.[17,18] In the present study, we identified the *GOLM1* as a *miR-143/145* cluster-regulated molecular target and proved that *miR-143/145* cluster directly binding 3′UTR of *GOLM1*. We also found that silencing of *GOLM1* resulted in significant inhibition of migration and invasion in PCa cells. Furthermore, overexpression of GOLM1 was observed in PCa clinical specimens, as detected by immunohistochemistry. These data suggested that GOLM1 functioned as an oncogene, contributing to cancer cell migration and invasion. However, the mechanisms mediating the overexpression of GOLM1 in PCa and its role in cancer cell migration and invasion remain unclear.

The GOLM1/GP73/GOLPH2 protein is encoded by the *GOLM1* gene, located on human chromosome 9q21.33. *GOLM1* contains two transcript variants, and both variants encode the same protein.[14] The expression of GOLM1 has been shown to be overexpressed in human PCa tissue,lung adenocarcinoma and hepatocellular carcinoma.[15–17,28,29] Structurally, GOLM1 resembles a type II Golgi transmembrane protein, and studies have shown that GOLM1 processes proteins synthesized in the rough endoplasmic reticulum and assists in the transport of protein cargo through the Golgi apparatus.[30] In PCa cells, GOLM1 is localized in the subapical cytoplasmic region, typical of Golgi distribution. Interestingly, the expression of GOLM1 is higher in the blood of patients with hepatocellular carcinoma and in the urine of patients with PCa than in healthy individuals, suggesting that GOLM1 is a useful tool for the diagnosis of human cancers.[14–17,29]

However, despite that a number of studies have demonstrated GOLM1 expression in cancers, we questioned whether GOLM1 contributed to the oncogenesis and metastasis of PCa. According to our immunohistochemistry data, there was no correlation between GOLM1 protein expression and tumor grade or stage. Even the gene expression data (GSE 29079) was not able to find clinical correlation. In contrast, another study reported the moderately increased expression of GOLM1 in prostatic intra-epithelial neoplasia, a precancerous condition.[15] This data suggested that GOLM1 contributes to the oncogenesis and progression of PCa. The clinical study with expression status of GOLM1 and clinical features of PCa will be necessary in future.

Multiple reports had indicated that the Golgi apparatus is a key player in cell migration and acts as a hub for different signaling pathways, including the mitogen-activated protein kinase pathway, the mammalian target of rapamycin pathway, Rho family GTPases and cyclin-dependent kinases, through signaling crucial molecules to translocate to and from the Golgi, thereby playing a key role in cell migration and invasion.[31,32] Therefore, elucidation of the regulatory networks of the Golgi apparatus will provide important information for the development of new therapeutic strategies against cancer cell metastasis. Further research is needed to reveal the oncogenic functions of GOLM1 that are regulated by the tumor-suppressive *miR-143/145* cluster in PCa. Therefore, improving our understanding of GOLM1 signaling, as mediated by the tumor-suppressive *miR-143/145* cluster, should shed light on the mechanisms of PCa oncogenesis and metastasis and assist in the development of more effective therapeutic intervention for this disease.

In conclusion, downregulation of the *miR-143/145* cluster is frequently observed in PCa clinical specimens. Restoration of these miRNAs significantly inhibited cancer cell migration and invasion, suggesting that *miR-143/145* functioned as a tumor suppressor in PCa. To the best of our knowledge, this is the first report

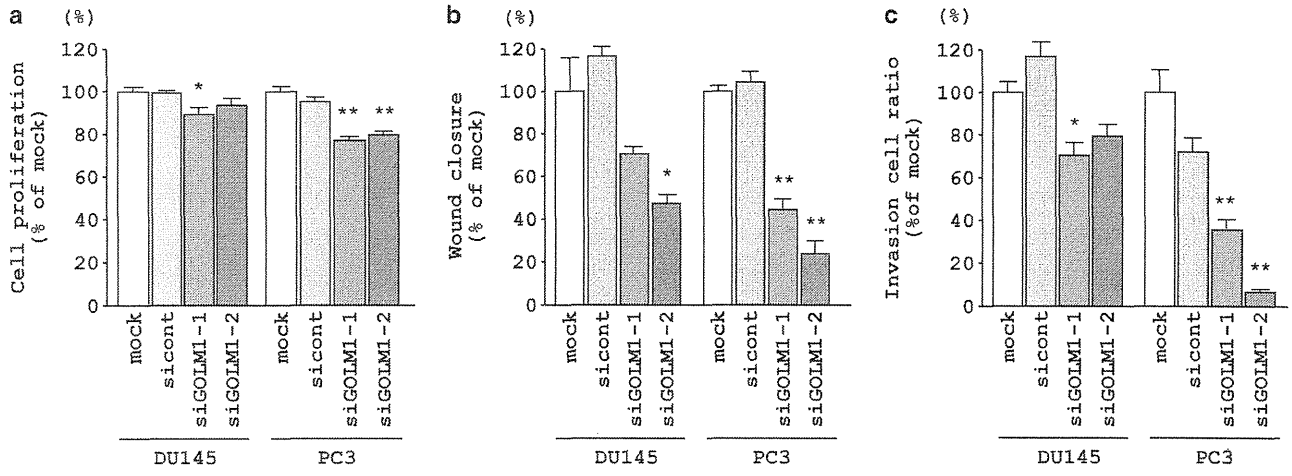

Figure 6 Effects of *GOLM1* silencing by si-GOLM1 transfection on the PCa cells. (a) Cell proliferation was determined by the XTT assay. (b) Cell migration activity was determined by the wound-healing assay. (c) Cell invasion activity was determined by the Matrigel invasion assay. $^{**}P<0.0001$, $^{*}P<0.01$.

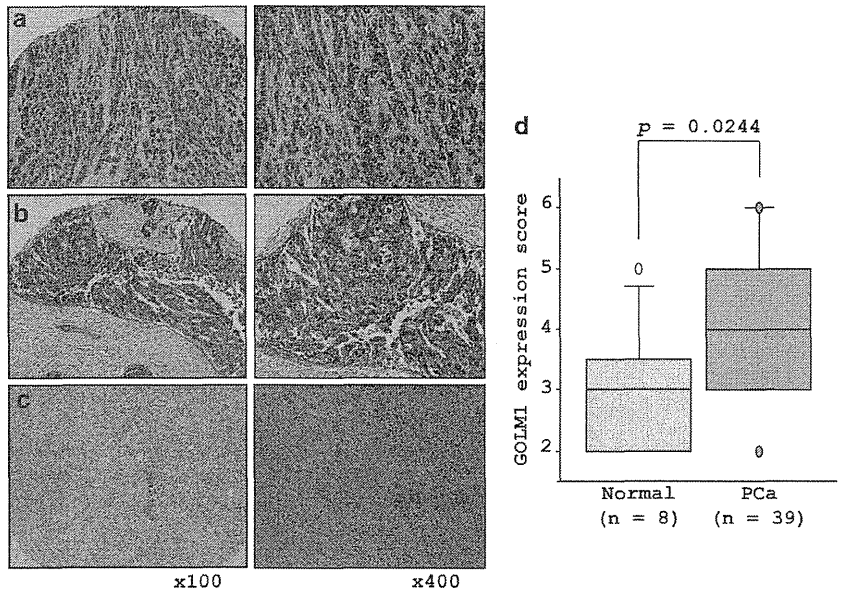

Figure 7 Immunohistochemical staining of GOLM1 in PCa ($n=39$) and normal prostate tissues ($n=8$) by tissue microarray (left panel, original magnification: ×100; right panel, original magnification: ×400). (a) A strongly stained tumor lesion (Gleason Score 4 + 5 = 9, pT3bN1M0). (b) A strongly stained tumor lesion (Gleason Score 4 + 5 = 9, pT3bN0M0). (c) Negative staining in normal, non-malignant prostate tissues. (d) Quantification of GOLM1 expression. The expression of GOLM1 was upregulated in PCa specimens compared with normal prostate tissues ($P=0.00244$).

demonstrating that the tumor-suppressive *miR-143/145* cluster directly regulated *GOLM1* in PCa cells. Moreover, GOLM1 was upregulated in PCa clinical specimens and contributed to cancer cell migration and invasion, indicating that this protein functioned as an oncogene. The identification of novel target oncogenes regulated by the *miR-143/145* cluster may lead to a better understanding of PCa oncogenesis and the development of new therapeutic strategies to treat this disease.

CONFLICT OF INTEREST

All the authors declare no conflict of interest.

ACKNOWLEDGEMENTS

This study was supported by the KAKENHI (C), 24592590 and (C), 23592351.

1 Siegel, R., Naishadham, D. & Jemal, A. Cancer statistics, 2013. *CA Cancer J. Clin.* **63**, 11–30 (2013).
2 Bott, S. R., Birtle, A. J., Taylor, C. J. & Kirby, R. S. Prostate cancer management: 2. An update on locally advanced and metastatic disease. *Postgrad. Med. J.* **79**, 643–645 (2003).
3 Timsit, M. O., Lebret, T. & Mejean, A. Chemotherapy of hormonorefractory and hormonoresistant metastatic prostate cancer. *Prog. Urol.* **18**(Suppl 7), S365–S375 (2008).
4 Carthew, R. W. & Sontheimer, E. J. Origins and mechanisms of miRNAs and siRNAs. *Cell* **136**, 642–655 (2009).
5 Filipowicz, W., Bhattacharyya, S. N. & Sonenberg, N. Mechanisms of post-transcriptional regulation by microRNAs: are the answers in sight? *Nat. Rev. Genet.* **9**, 102–114 (2008).
6 Friedman, R. C., Farh, K. K., Burge, C. B. & Bartel, D. P. Most mammalian mRNAs are conserved targets of microRNAs. *Genome Res.* **10**, 92–105 (2009).
7 Hobert, O. Gene regulation by transcription factors and microRNAs. *Science* **319**, 1785–1786 (2008).

8 Iorio, M. V. & Croce, C. M. MicroRNAs in cancer: small molecules with a huge impact. *J. Clin. Oncol.* **27,** 5848–5856 (2009).
9 Fuse, M., Kojima, S., Enokida, H., Chiyomaru, T., Yoshino, H., Nohata, N. *et al.* Tumor suppressive microRNAs (miR-222 and miR-31) regulate molecular pathways based on microRNA expression signature in prostate cancer. *J. Hum. Genet.* **57,** 691–699 (2012).
10 Kano, M., Seki, N., Kikkawa, N., Fujimura, L., Hoshino, I., Akutsu, Y. *et al.* miR-145, miR-133a and miR-133b: tumor suppressive miRNAs target FSCN1 in esophageal squamous cell carcinoma. *Int. J. Cancer* **127,** 2804–2814 (2010).
11 Fuse, M., Nohata, N., Kojima, S., Sakamoto, S., Chiyomaru, T., Kawakami, K. *et al.* Restoration of miR-145 expression suppresses cell proliferation, migration and invasion in prostate cancer by targeting FSCN1. *Int. J. Oncol.* **38,** 1093–1101 (2011).
12 Huang, S., Guo, W., Tang, Y., Ren, D., Zou, X. & Peng, X. miR-143 and miR-145 inhibit stem cell characteristics of PC-3 prostate cancer cells. *Oncol. Rep.* **28,** 1831–1837 (2012).
13 Guo, W., Ren, D., Chen, X., Tu, X., Huang, S., Wang, M. *et al.* HEF1 promotes epithelial mesenchymal transition and bone invasion in prostate cancer under the regulation of microRNA-145. *J. Cell Biochem.* **114,** 1606–1615 (2013).
14 Kim, H. J., Lv, D., Zhang, Y., Peng, T. & Ma, X. Golgi phosphoprotein 2 in physiology and in diseases. *Cell Biosci.* **2,** 31 (2012).
15 Varambally, S., Laxman, B., Mehra, R., Cao, Q., Dhanasekaran, S. M., Tomlins, S. A. *et al.* Golgi protein GOLM1 is a tissue and urine biomarker of prostate cancer. *Neoplasia* **10,** 1285–1294 (2008).
16 Kristiansen, G., Fritzsche, F. R., Wassermann, K., Jager, C., Tolls, A., Lein, M. *et al.* GOLPH2 protein expression as a novel tissue biomarker for prostate cancer: implications for tissue-based diagnostics. *Br. J. Cancer* **99,** 939–948 (2008).
17 Li, W., Wang, X., Li, B., Lu, J. & Chen, G. Diagnostic significance of overexpression of Golgi membrane protein 1 in prostate cancer. *Urology* **80,** 952 e1-7 (2012).
18 Yoshino, H., Chiyomaru, T., Enokida, H., Kawakami, K., Tatarano, S., Nishiyama, K. *et al.* The tumour-suppressive function of miR-1 and miR-133a targeting TAGLN2 in bladder cancer. *Br. J. Cancer* **104,** 808–818 (2011).
19 Nohata, N., Hanazawa, T., Kikkawa, N., Sakurai, D., Fujimura, L., Chiyomaru, T. *et al.* Tumour suppressive microRNA-874 regulates novel cancer networks in maxillary sinus squamous cell carcinoma. *Br. J. Cancer* **105,** 833–841 (2011).
20 Brase, J. C., Johannes, M., Mannsperger, H., Falth, M., Metzger, J., Kacprzyk, L. A. *et al.* TMPRSS-ERG-specific transcriptional modulation is associated with prostate cancer biomarkers and TGF-β signaling. *BMC Cancer* **11,** 507 (2011).
21 Kojima, S., Chiyomaru, T., Kawakami, K., Yoshino, H., Enokida, H., Nohata, N. *et al.* Tumour suppressors miR-1 and miR-133a target the oncogenic function of purine nucleoside phosphorylase (PNP) in prostate cancer. *Br. J. Cancer* **106,** 405–413 (2012).
22 Jain, A. K., Allton, K., Iacovino, M., Mahen, E., Milczarek, R. J., Zwaka, T. P. *et al.* p53 regulates cell cycle and microRNAs to promote differentiation of human embryonic stem cells. *PLoS Biol.* **10,** e1001268 (2012).
23 Sachdeva, M., Zhu, S., Wu, F., Wu, H., Walia, V., Kumar, S. *et al.* p53 represses c-Myc through induction of the tumor suppressor miR-145. *Proc. Natl Acad. Sci. USA* **106,** 3207–3212 (2009).
24 Kent, O. A., Chivukula, R. R., Mullendore, M., Wentzel, E. A., Feldmann, G., Lee, K. H. *et al.* Repression of the miR-143/145 cluster by oncogenic Ras initiates a tumor-promoting feed-forward pathway. *Genes Dev.* **24,** 2754–2759 (2010).
25 Sachdeva, M. & Mo, Y. Y. miR-145-mediated suppression of cell growth, invasion and metastasis. *Am. J. Transl. Res.* **2,** 170–180 (2010).
26 Yoshino, H., Seki, N., Itesako, T., Chiyomaru, T., Nakagawa, M. & Enokida, H. Abberant expression of microRNAs in bladder cancer. *Nat. Rev. Urol.* **10,** 396–404 (2013).
27 Yoshino, H., Enokida, H., Itesako, T., Kojima, S., Kinoshita, T., Tatarano, S. *et al.* The tumor-suppressive *microRNA-143/145* cluster targets hexokinase-2 in renal cell carcinoma. *Cancer Sci.* doi:10.1111/cas.12282 (2013).
28 Zhang, F., Gu, Y., Li, X., Wang, W., He, J. & Peng, T. Up-regulated Golgi phosphoprotein 2 (GOLPH2) expression in lung adenocarcinoma tissue. *Clin. Biochem.* **43,** 983–991 (2010).
29 Bachert, C., Fimmel, C. & Linstedt, A.D. Endosomal trafficking and proprotein convertase cleavage of cis Golgi protein GP73 produces marker for hepatocellular carcinoma. *Traffic* **8,** 1415–1423 (2007).
30 Kladney, R. D., Bulla, G. A., Guo, L., Mason, A. L., Tollefson, A. E., Simon, D. J. *et al.* GP73, a novel Golgi-localized protein upregulated by viral infection. *Gene* **249,** 53–65 (2000).
31 Migita, T. & Inoue, S. Implications of the Golgi apparatus in prostate cancer. *Int. J. Biochem. Cell Biol.* **44,** 1872–1876 (2012).
32 Millarte, V. & Farhan, H. The Golgi in cell migration: regulation by signal transduction and its implications for cancer cell metastasis. *ScientificWorldJournal* **2012,** 498278 (2012).

Supplementary Information accompanies the paper on Journal of Human Genetics website (http://www.nature.com/jhg)

Cancer Science
The official journal of the Japanese Cancer Association JCA

Gene expression signature-based prognostic risk score in patients with glioblastoma

Atsushi Kawaguchi,[1] Naoki Yajima,[2] Naoto Tsuchiya,[2] Jumpei Homma,[2] Masakazu Sano,[2] Manabu Natsumeda,[2] Hitoshi Takahashi,[3] Yukihiko Fujii,[2] Tatsuyuki Kakuma[1] and Ryuya Yamanaka[4,5]

[1]Biostatistic Center, Kurume University School of Medicine, Kurume; Departments of [2]Neurosurgery, [3]Pathology, Brain Research Institute, Niigata University, Niigata; [4]Graduate School for Health Care Science, Kyoto Prefectural University of Medicine, Kyoto, Japan

(Received January 21, 2013/Revised May 22, 2013/Accepted May 29, 2013/Accepted manuscript online June 7, 2013/Article first published online July 5, 2013)

The present study aimed to identify genes associated with patient survival to improve our understanding of the underlying biology of gliomas. We investigated whether the expression of genes selected using random survival forests models could be used to define glioma subgroups more objectively than standard pathology. The RNA from 32 non-treated grade 4 gliomas were analyzed using the GeneChip Human Genome U133 Plus 2.0 Expression array (which contains approximately 47 000 genes). Twenty-five genes whose expressions were strongly and consistently related to patient survival were identified. The prognosis prediction score of these genes was most significant among several variables and survival analyses. The prognosis prediction score of three genes and age classifiers also revealed a strong prognostic value among grade 4 gliomas. These results were validated in an independent samples set (n = 488). Our method was effective for objectively classifying grade 4 gliomas and was a more accurate prognosis predictor than histological grading. (*Cancer Sci* 2013; 104: 1205–1210)

Glioblastomas are pathologically the most aggressive form of glioma, with a median survival range of only 9–15 months.[1,2] Even advances in cancer biology, surgical techniques, chemotherapy and radiotherapy have led to little improvement in survival rates of glioblastoma patients.[1] Poor prognosis is attributable to difficulties in early detection and to a high recurrence rate after initial treatment. Therefore, more effective therapeutic approaches, a clearer understanding of the biological features of glioblastoma and the identification of novel target molecules are needed for improved diagnosis and therapy of this disease.

Several histological grading schemes exist. The World Health Organization (WHO) system is currently the most widely used; a high WHO grade correlates with clinical progression and decreased survival rate.[3] However, individual fates vary within diagnostic categories, even in grade 4 glioma,[1,2] indicating the need for additional prognostic markers. The inadequacy of histopathological grading is evidenced, in part, by the inability to recognize patients prospectively.

Microarray technology has permitted the development of multiorgan cancer classification including gliomas, the identification of glioma subclasses, the discovery of molecular markers and predictions of disease outcomes.[4–14] Unlike clinicopathological staging, molecular staging can predict long-term outcomes of individuals based on gene expression profiles of tumors at diagnosis, enabling clinicians to make optimal clinical decisions. The analysis of gene expression profiles in clinical materials is an essential step towards clarifying the detailed mechanisms of oncogenesis and the discovery of target molecules for the development of novel therapeutic drugs.

In the present study, we describe an expression profiling study of a panel of 32 patients with grade 4 gliomas for the identification of genes that predict overall survival (OS) using random survival forests models, with validation in independent data sets.

Materials and Methods

Samples. Tissues were snap-frozen in liquid nitrogen within 5 min of harvesting and stored thereafter at −80°C. The clinical stage was estimated from accompanying surgical pathology and clinical reports. Samples were specifically re-reviewed by a board-certified pathologist at Niigata University, Niigata, Japan according to WHO criteria, by observing sections of paraffin-embedded tissues that were adjacent or in close proximity to frozen samples from which the RNA was subsequently extracted. The histopathology of each collected specimen was reviewed to confirm the adequacy of the sample (i.e. minimal contamination with non-neoplastic elements) and to assess the extent of tumor necrosis and cellularity. Informed consent was obtained from all patients for the use of the samples, in accordance with the guidelines of the Ethical Committee on Human Research, Niigata University Medical School (Protocol #70). Overall survival was measured from the date of diagnosis. Survival end-points corresponded to the dates of death or last follow up.

RNA extraction and array hybridization. Approximately 100 mg of tissue from each tumor was used to extract total RNA using the Isogen method (Nippongene, Toyama, Japan) following the manufacturer's instructions. The quality of RNA obtained was verified with the Bioanalyzer System (Agilent Technologies, Tokyo, Japan) using RNA Pico Chips. Only samples with 28S/18S ratios >0.7 and with no evidence of ribosomal peak degradation were included in the present study. One microgram of each RNA was processed for hybridization using GeneChip Human Genome U133 Plus 2.0 Expression arrays (Affymetrix, Inc., Tokyo, Japan), which comprised approximately 47 000 genes. After hybridization, the chips were processed using a Fluidics Station 450, a High-Resolution Microarray Scanner 3000 and a GCOS Workstation Version 1.3 (Affymetrix, Inc).

Validation of differential expression using real-time quantitative PCR. The quantitative PCR (QPCR) was performed using a StepOne Real-Time PCR System (Applied Biosystems, Tokyo, Japan) and TaqMan Universal PCR Master Mix (Applied Biosystems) according to the manufacturer's protocol. The Assays-on-Demand probe/primer sets (Applied Biosystems) used were as follows: ANGPTL1, Hs00559786_m1; ARHGAP39, Hs00286798_m1; ASF1A, Hs00204044_m1;

[5]To whom correspondence should be addressed.
E-mail: ryaman@cmt.kpu-m.ac.jp

doi: 10.1111/cas.12214

CASP8, Hs01018151_m1; C11orf71, Hs00535489_s1; EFNB2, Hs00187950_m1; GAPDH, Hs99999905_m1; GPNMB, Hs01095679_m1; ITGA7, Hs00174397_m1; LDHA, Hs00855332_g1; LMAN2L, Hs01091681_m1; LOXL3, Hs01046945_m1; MED29, Hs00378316_m1; and MGMT, Hs01037698_m1.

Total RNA (1 μg) was reverse transcribed into cDNA using SuperScript II (Invitrogen, Tokyo, Japan) and 1 μL of the resulting cDNA was used for QPCR. Validation was performed on a subset of tumors that were part of the original tumor data set assessed. Assays were carried out in duplicate. The raw data produced using the QPCR referred to the number of cycles required for reactions to reach the exponential phase. Expression of GAPDH was used to normalize the QPCR data. Mean expression fold change differences between tumor groups were calculated using the $2^{-\Delta\Delta CT}$ method.[15]

Immunohistochemistry. Five-micron sections from formalin-fixed, paraffin-embedded tissue specimens were used for immunohistochemistry (IHC). Endogenous peroxidase was blocked with 0.3% H_2O_2 in methanol. Antigen retrieval was performed by autoclaving at 120°C for 10 min in 50 mM citrate buffer (pH 6.0). The IHC for anti-O6-methylguanine-methyltransferase (MGMT; antibody dilution 1:50; clone MT3.1; Millipore, Billerica, MA, USA) was performed as described previously.[16] Immunoreactivity (MGMT staining index [SI]) was quantified by counting stained tumor nuclei in >1000 cells and was expressed as a percentage of positive cells. A MGMT SI >30% was considered positive for MGMT. Averages of three independent measurements were calculated to the first decimal place. Observers were not aware of case numbers.

Analysis of the isocitrate dehydrogenase 1 (IDH1) codon 132 mutation. A 129-bp fragment of IDH1 that included codon 132 was amplified using IDH1f, 5′-CGGTCTTCAGAGAAG CCATT-3′ as the sense primer and IDH1r, 5′-GCAAAATCA CATTATTGCCAAC-3′ as the antisense primer. A PCR was performed on 20 ng of DNA with Taq DNA Polymerase (Takara, Tokyo, Japan) and standard conditions of 35 cycles were used. The PCR amplification product was sequenced using a BigDyeTerminator v3.1 Sequencing Kit (Applied Biosystems) using the sense primer IDH1f and antisense primer IDH1rc, 5′-TTCATACCTTGCTTAATGGGTGT-3′. Sequences were determined using the semiautomated sequencer (ABI 3100 Genetic Analyzer; Applied Biosystems) and Sequence Pilot version 3.1 software (JSI-Medisys, Kippenheim, Germany) as described previously.[17]

Bioinformatics analysis. All statistical analyses were performed using R software[18] and Bioconductor.[19] The Affymetrix GeneChip probe-level data were preprocessed using MAS 5.0 (Affymetrix Inc.) for background adjustment and log-transformation (base 2). Each array was normalized using a quantile normalization to impose the same empirical distribution of intensities to each array. Genes that passed the filter criteria below were considered for further analysis. To select predictors (genes) for OS, we first set filtered gene expressions and applied the random survival forests–variable hunting (RSF-VH) algorithm.[20] Among the algorithm parameters, the number of Monte Carlo iterations (nrep) and value to control step size used in the forward process (nstep) were set as nrep = 100 and nstep = 5, respectively, following the method of Ishwaran *et al.*[20] For other parameters such as number of trees and number of variables selected randomly at each node, we used the default settings for varSelfunction within the RandomSurvivalForest package before selection. We classified samples into two survival groups using Ward's minimum variance cluster analysis, inputting ensemble cumulative hazard functions for each individual for all unique death time-points estimated from the fitted random survival forests model to selected genes.

The two classified survival groups were used to compute the prognosis prediction score (PPS) from a simple form (linear combination of gene expressions). To do this, we used principal component analysis and receiver operating characteristic

Table 1. Patient characteristics of grade 4 glioma

Variable	Test set (n = 32)	Validation set (n = 488)	P
Age (years)			
Average	54.5	55.0	0.84
Range	18–80	10–86	
Gender			
Male	20	305	1.00
Female	12	183	
Survival time (days)	411	364	0.41

Table 2. Identification of survival related 25 genes

Probe	Symbol	Description	VI
225708_at	MED29	Mediator complex subunit 29	0.0202
217939_s_at	AFTPH	Aftiphilin	0.0101
227876_at	ARHGAP39	Rho GTPase activating protein 39	0.0101
228821_at	ST6GAL2	ST6 beta-galactosamide alpha-2,6-sialyltranferase 2	0.0101
200650_s_at	LDHA	Lactate dehydrogenase A	0.0081
220260_at	TBC1D19	TBC1 domain family, member 19	0.0060
218981_at	ACN9	ACN9 homolog (*S. cerevisiae*)	0.0060
231773_at	ANGPTL1	Angiopoietin-like 1	0.0060
201141_at	GPNMB	Glycoprotein (transmembrane) nmb	0.0040
228255_at	ALS2CR4	Amyotrophic lateral sclerosis 2 (juvenile) chromosome region, candidate 4	0.0040
203427_at	ASF1A	ASF1 anti-silencing function 1 homolog A (*S. cerevisiae*)	0.0020
222108_at	AMIGO2	Adhesion molecule with Ig-like domain 2	0.0020
1562527_at	LOC283027	Hypothetical protein LOC283027	0.0000
218789_s_at	C11orf71	Chromosome 11 open reading frame 71	0.0000
219240_s_at	C10orf88	Chromosome 10 open reading frame 88	−0.0020
213373_s_at	CASP8	Caspase 8, apoptosis-related cysteine peptidase	−0.0020
225126_at	MRRF	Mitochondrial ribosome recycling factor	−0.0020
209663_s_at	ITGA7	Integrin, alpha 7	−0.0040
223222_at	SLC25A19	Solute carrier family 25 (mitochondrial thiamine pyrophosphate carrier), member 19	−0.0040
214271_x_at	RPL12	Ribosomal protein L12	−0.0040
229648_at	ARHGAP32	Rho GTPase activating protein 32	−0.0040
228253_at	LOXL3	Lysyl oxidase-like 3	−0.0060
202669_s_at	EFNB2	Ephrin-B2	−0.0081
206172_at	IL13RA2	Interleukin 13 receptor, alpha 2	−0.0101
221274_s_at	LMAN2L	Lectin, mannose-binding 2 like	−0.0141

VI, variable importance.

doi: 10.1111/cas.12214

analysis. Briefly, we computed the first principal component of gene expressions selected by the RSF-VH algorithm as a risk score and then searched for the optimal value to predict survival groups with maximum accuracy using the Youden index.[21] Validation for this method is used in the validation set ($n = 488$; Table 1), which is derived from glioblastoma patients in four external data sets.[8,10,12,22]

The survival tree method[23] constructs prognostic groups based on PPS and age among those with grade 4 glioma. This method is based on a recursive partition of the PPS and age values while splitting patients into the subset. Final output results in groups of patients with similar prognoses, which are represented as combinations of binarized PPS or age. This was executed using the rpart package of the R software.

The Kaplan–Meier method was used to estimate the survival distribution for each group. A log-rank test was used to test differences between survival groups. The association of the PPS with OS was evaluated using multivariate analyses with clinical characteristics and with other predictors using the Cox proportional hazards regression model. $P < 0.05$ was considered statistically significant.

Results

Patient characteristics. Thirty-two non-treated primary glioblastomas (WHO grade IV) came from patients who underwent surgical resections between 2000 and 2005 (Table 1). The median age of patients was 54.5 years (range, 18–80 years). Twenty patients were male and 12 were female. The preoperative Karnofsky performance status (KPS) was at least 70 in 25 (78%) patients. The IDH1 mutation was negative in 31 cases, but was detected in one patient who remains alive 2365 days after the onset of disease. The MGMT IHC was positive in 21 cases and negative in 11 cases. After maximum surgical tumor resections, patients received external beam radiation therapy (standard dose of 60 Gy to the tumor with a 2-cm margin) and first-line chemotherapy with nimustine and temozolomide at recurrence. Patients were monitored for tumor recurrence during initial and maintenance therapy using MRI or computed tomography. Treatments were carried out at the Department of Neurosurgery, Niigata University Hospital. The median survival time was 13.7 months.

Selection of predictive genes. Microarray data were deposited in the Gene Expression Omnibus (accession number GSE 43378) and 25 genes were selected as predictors. Table 2 shows a list of the genes with their variable importance values. The scatter plot in Supporting Information Figure S1 shows the relationships between the estimated ensemble mortalities and expression for six selected genes (*AFTPH, ARHGAP39, CASP8, ITGA7, LDHA* and *LOXL3*). Validation of the microarray results was accomplished using QPCR. These 10 genes were also found to be differentially expressed between short-term (survival time, ≤1.5 years) and long-term (survival time, ≥2.5 years) survivors (Table S1). The heat map (Fig. S2) shows patients clustered by estimated ensemble mortalities (columns) and genes clustered by their expression levels (rows). For patients with low survival (blue bar), the lower genes are overexpressed while the upper genes are underexpressed. For patients with improved survival (red bar), these patterns were reversed; thus, the indicated genes might be effective in distinguishing between patients with different survival rates.

Identification of a PPS associated with survival. The gene expression predictor PPS was computed from a linear combination of the 25 genes and was calculated for each tumor as

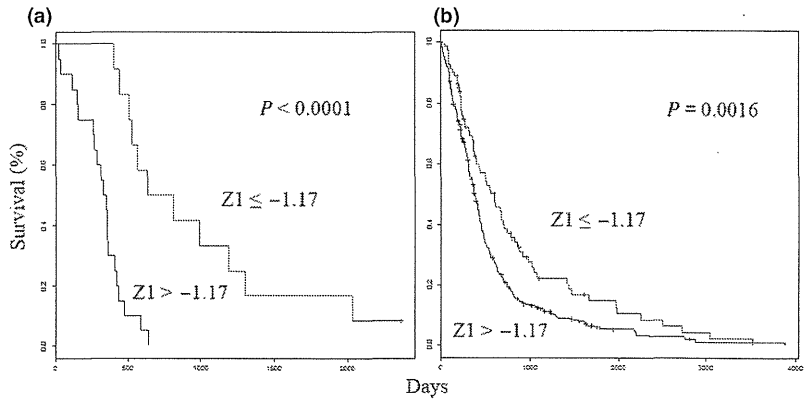

Fig. 1. Survival analyses using the selected 25-gene classifiers show the prognostic value for glioblastoma. Kaplan–Meier curves that compare groups classified using the Z_1 prognosis prediction score with the 25-gene model in the test (a) and validation (b) sets.

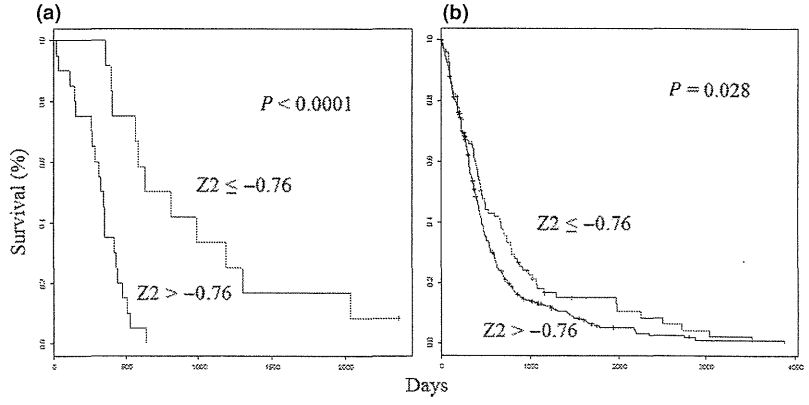

Fig. 2. Survival analyses using the selected three-gene classifiers show the prognostic value for glioblastoma. Kaplan–Meier curves that compare groups classified using the Z_2 prognosis prediction score with the three-gene model in the test (a) and validation (b) sets.

follows:

$$Z_1 = 0.27 \times GPNMB + 0.09 \times EFNB2 - 0.22 \times ASF1A + 0.02 \times LOC283027 + 0.15 \times AMIGO2 + 0.22 \times IL13RA2 + 0.25 \times ITGA7 + 0.15 \times LDHA - 0.01 \times C11orf71 + 0.15 \times AFTPH + 0.15 \times TBC1D19 - 0.21 \times MED29 + 0.02 \times ACN9 + 0.29 \times SLC25A19 + 0.16 \times RPL12 - 0.09 \times ALS2CR4 - 0.14 \times C10orf88 - 0.11 \times ARHGAP39 + 0.18 \times LMAN2L + 0.29 \times CASP8 - 0.28 \times ST6GAL2 + 0.33 \times LOXL3 + 0.08 \times ANGPTL1 + 0.22 \times MRRF - 0.33 \times ARHGAP32.$$

The Z_1 score of the expression value for each individual gene was adapted in this formula. The Z_1 scores ranged from −4.91 to 4.28, with high scores associated with poor outcomes. The optimal cut-off was a Z score of −1.17. As expected, the predictor performed well in terms of patient prognosis; the improved prognosis group ($Z \leq -1.17$) had a median survival time of 721 days, while the poor prognosis group ($Z > -1.17$) had a significantly lower median survival time of 335 days ($P < 0.0001$; Fig. 1a).

Identification of a PPS with a three-gene set associated with survival. For more practical purposes, the gene expression predictor PPS was computed from a linear combination of three genes and was calculated for each tumor as follows:

Table 3. Prognostic value of clinical factors stratified by overall survival (OS) in patients with grade 4 glioma

Variable	*n*	Median OS (days)	*P*
Age (years)			
≥60	17	352	<0.05
<60	15	525	
Gender			
Male	20	434	0.48
Female	12	337	
KPS			
≥70	25	474	<0.01
<70	7	268	
IDH1			
Wild	31	405	0.05
Mutated	1	N.D.	
MGMT IHC			
Positive	21	352	0.09
Negative	11	630	
MGMT mRNA			
>0.017	16	407	0.42
≤0.017	16	419	
Subtype			
CL	7	432	0.009
MES	11	308	
NL	7	988	
PN	7	417	
Z_1 Score			
>−1.17	20	335	<0.0001
≤−1.17	12	721	
Z_2 Score			
>−0.76	20	335	<0.0001
≤−0.76	12	721	

CL, classical; IDH1, isocitrate dehydrogenase 1; IHC, immunohistochemistry; KPS, Karnofsky performance status; MES, mesenchymal; MGMT, O6-methylguanine-methyltransferase; ND, not determined; NL, neural; PN, proneural.

$$Z_2 = -0.63 \times ASF1A + 0.62 \times ITGA7 + 0.47 \times AFTPH$$

The Z_2 score of the expression value for each individual gene was adapted in this formula. The Z_2 scores ranged from −2.53 to 2.27, with high scores associated with poor outcomes. The optimal cut-off was a Z score of −0.76. As expected, the predictor performed well in terms of patient prognosis; the improved prognosis group ($Z \leq -0.76$) had a median survival time of 721 days, while the poor prognosis group ($Z > -0.76$) had a significantly lower median survival time of 335 days ($P < 0.0001$; Fig. 2a). Classification using cell-of-origin is associated with survival. We classified our cases into proneural, neural, classical and mesenchymal subtypes using a gene expression-based method according to Verhaak *et al.*[13] (Fig. S3A). These four groups differed significantly in survival rates ($P = 0.0093$; Fig. S3B) and classification by cell-of-origin was found to be significantly associated with patient survival.

The gene expression predictor is the most significant feature. The Z PPS results were compared with traditional individual indicators. As shown in Table 3, Z_1, Z_2, age, KPS and subtype were significantly associated with OS in univariate analyses. Table 4 shows the results of the multivariate analyses, which found that the gene expression predictor Z_1 was significantly associated with OS. The PPS was the most significant feature of these clinical parameters.

The PPS formula was validated in the independent sample set. The PPS formula was validated in the validation set ($n = 488$; Table 1), which is derived from glioblastoma patients in four external data sets.[8,10,12,22] The Z_1 scores ranged from −5.43 to 5.33. As expected, the OS was significantly higher in the improved prognosis group ($Z \leq -1.17$) than in the poor prognosis group ($Z > -1.17$; $P = 0.0016$; Fig. 1b). The Z_2 scores ranged from −3.98 to 2.66. As expected, the OS was significantly higher in the improved prognosis group ($Z \leq -0.76$) than in the poor prognosis group ($Z > -0.76$; $P = 0.028$; Fig. 2b).

Survival analyses using the PPS with a three-gene set and age classifiers shows a prognostic value for patients with grade 4 glioma. Even among Grade 4 gliomas in both test ($n = 32$) and validation sets ($n = 488$), the OS ranged between 0 and 3880 days. Fifty-two patients (10%) survived for longer than 1000 days. As predicted by the survival tree, the OS differed significantly between the improved prognosis group ($-0.76 \geq Z_2$ or $-0.76 < Z_2$ with age <57 years) and the poor prognosis group ($-0.76 < Z_2$ with age ≥57 years) in the test and validation set ($P = 0.0006$ and $P < 0.0001$, respectively; Fig. 3). The median OS using test and validation data sets was 641 and 490 days, respectively, for the improved prognosis group and 347 and 302 days, respectively, for the poor prog-

Table 4. Multivariate analysis: prognosis prediction score and clinical and therapeutic variables associated with overall survival in patients with grade 4 glioma

Variable	Subgroup	Entire series ($n = 32$)		
		Hazard ratio	95% CI	*P*
Z_1	Continuous variable	1.34	1.03–1.77	0.026
Z_2	Continuous variable	1.48	0.95–2.38	0.081
MGMT IHC	Positive/Negative	1.72	0.70–4.30	0.228
Age (years)	≥60, <60	2.22	0.95–5.37	0.065
KPS	≥70, <70	2.76	0.88–8.50	0.078

CI, confidence interval; IHC, immunohistochemistry; MGMT, anti-O6-methylguanine-methyltransferase.

doi: 10.1111/cas.12214

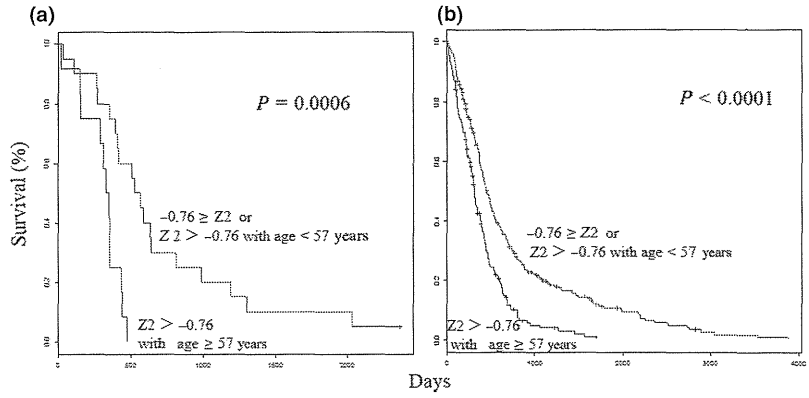

Fig. 3. Survival analyses using the Z_2 prognosis prediction score (PPS) and age classifiers reveal a prognostic value for glioblastoma. Kaplan–Meier curves compare groups classified using the Z_2 PPS and age in the test (a) and validation (b) sets.

nosis group. The two-year survival rates were 36.3% and 30.8% in the improved prognosis group and 4.7% and 11.8% in the poor prognosis group, using the test and validation data sets, respectively.

Discussion

We assessed relationships between gene expression and survival time using a random survival forests model. This is classified into a tree-based method, which aids the detection of interactions. As discussed by Cordell, the functional form should contain gene-by-gene interaction terms.[24] The model was developed for use with datasets in which several variables (genes, in the present case) greatly outnumber patients; a framework of random forests is needed for such an analysis. Genes were selected using the RSF-VH algorithm, which eliminates the need to screen the genes.[20]

Many studies of microarray data use univariate analyses for screening in which potential genes that interact with other genes may be dropped from the analyses. However, the RSF-VH algorithm is more appropriate for our application and we previously reported its usefulness[20] in the identification of a gene-expression signature that predicts outcomes in patients with malignant glioma and primary central nervous system lymphoma.[14,25]

Although our predictor was mainly based on cases from first-line nitrosourea-based chemotherapy, results from the combined four external data sets,[8,10,12,22] in which first-line temozolomide-based chemotherapy was used, support the universal performance of the predictor, irrespective of the chemotherapeutic regimen. Survival benefit by chemotherapy is relatively small in most grade 4 gliomas, so it is important to elucidate the differences in the intrinsic biological characteristics of the tumors. Genetic differences within malignant gliomas also underscore the heterogeneity of these tumor types. Compared with our previous report of oligodendrocytic tumor patients,[14] three (*GPNMB, LOXL3* and *IL13RA2*) out of 25 genes are identical to the present study.

The value of gene expression-based predictors in estimating the prognosis of malignant glioma patients will not be fully realized until more efficacious therapies are available for those in whom current treatment is less successful. In this regard, although the biological investigation of these genes is important, expression profiles might predict long-term survival as well as yielding clues about individual genes involved in tumor development, progression and response to therapy. Moreover, the ability to distinguish between histologically ambiguous gliomas will enable appropriate therapies to be tailored to specific tumor subtypes. Class prediction models based on defined molecular profiles allow the classification of malignant gliomas in a manner that will better correlate with clinical outcomes than with standard pathology. Glioblastomas have wide-ranging survival times, which require a more precise prognostic scoring system to study novel therapeutic approaches. Therefore, the identification of molecular subclasses could greatly facilitate prognosis and our ability to develop effective treatment protocols. As our PPS involves a small number of genes, quantitative reverse transcriptase PCR assays or customized DNA microarrays could be developed for clinical applications. Molecular targeted therapies that specifically target disabled pathways might then be tailored for those patients with poor prognoses.

In summary, we identified gene signatures associated with outcome in patients with glioblastoma. Adaptation of subsets of these genes for use in clinical assays could result in improved outcome prediction. We have extended our observations to validate these signatures using independent data sets from other institutions. Our profiling results should help construct a new classification scheme that better assesses clinical malignancies compared with the conventional histological classification system.

Acknowledgments

This work was supported in part by JSPS KAKENHI grant number 21700312 to A.K. and 17390394 to R.Y.

Disclosure Statement

The authors have no conflict of interest.

References

1 Stewart LA. Chemotherapy in adult high-grade glioma: a systematic review and meta-analysis of individual patient data from 12 randomised trials. *Lancet* 2002; **359**: 1011–8.

2 Stupp R, Hegi ME, Mason WP *et al.* Effects of radiotherapy with concomitant and adjuvant temozolomide versus radiotherapy alone on survival in glioblastoma in a randomised phase III study: 5-year analysis of the EORTC–NCIC trial. *Lancet Oncol* 2009; **10**: 459–66.

3 Kleihues P, Louis DN, Wiestler OD *et al.* WHO grading of tumours of the central nervous system. In: Louis DN, Ohgaki H, Wiestler OD, Cavenee WK, eds. *World Health Organization Classification of Tumours of the Nervous System*. Lyon, France: IARC Press, 2007; 10–11.

4 van de Vijver MJ, He YD, van't Veer LJ *et al.* A gene-expression signature as a predictor of survival in breast cancer. *N Engl J Med* 2002; **347**: 1999–2009.

5 Godard S, Getz G, Delorenzi M *et al.* Classification of human astrocyticgliomas on the basis of gene expression: a correlated group of genes with angio-

genic activity emerges as a strong predictor of subtypes. *Cancer Res* 2003; **63**: 6613–25.
6 Nutt CL, Mani DR, Betensky RA *et al.* Gene expression-based classification of malignant gliomas correlates better with survival than histological classification. *Cancer Res* 2003; **63**: 1602–7.
7 Sorlie T, Tibshirani R, Parker J *et al.* Repeated observation of breast tumor subtypes in independent gene expression data sets. *Proc Natl Acad Sci USA* 2003; **100**: 8418–23.
8 Freije WA, Castro-Vargas FE, Fang Z *et al.* Gene expression profiling of gliomas strongly predicts survival. *Cancer Res* 2004; **64**: 6503–10.
9 Rich JN, Hans C, Jones B *et al.* Gene expression profiling and genetic markers in glioblastoma survival. *Cancer Res* 2005; **65**: 4051–8.
10 Phillips HS, Kharbanda S, Chen R *et al.* Molecular subclasses of high-grade glioma predict prognosis, delineate a pattern of disease progression, and resemble stages in neurogenesis. *Cancer Cell* 2006; **9**: 157–73.
11 Yamanaka R, Arao T, Yajima N *et al.* Identification of expressed genes characterizing long-term survival in malignant glioma patients. *Oncogene* 2006; **25**: 5994–6002.
12 Petalidis LP, Oulas A, Backlund M *et al.* Improved grading and survival prediction of human astrocytic brain tumors by artificial neural network analysis of gene expression microarray data. *Mol Cancer Ther* 2008; **7**: 1013–24.
13 Verhaak RGW, Hoadley KA, Purdom E *et al.* Integrated genomic analysis identifies clinically relevant subtypes of glioblastoma characterized by abnormalities in PDGFRA, IDH1, EGFR, and NF1. *Cancer Cell* 2010; **17**: 98–110.
14 Kawaguchi A, Yajima N, Komohara Y *et al.* Identification and validation of a gene expression signature that predicts outcome in malignant glioma patients. *Int J Oncol* 2012; **40**: 721–30.
15 Livak KJ, Schmittgen TD. Analysis of relative gene expression data using real-time quantitative PCR and the 2(-Delta Delta C(T)) Method. *Methods* 2001; **25**: 402–8.
16 Nakasu S, Fukami T, Baba K, Matsuda M. Immunohistochemical study for O6-methylguanine-DNA methyltransferase in the non-neoplastic and neoplastic components of gliomas. *J Neurooncol* 2004; **70**: 333–40.
17 Balss J, Meyer J, Mueller W *et al.* Analysis of the IDH1 codon 132 mutation in brain tumors. *Acta Neuropathol* 2008; **116**: 597–602.
18 R Development Core Team. *R: A Language and Environment for Statistical Computing*. Vienna, Austria: R Foundation for Statistical Computing, 2011. [Cited 10 Dec 2012.] Available from URL: http://www.R-project.org.
19 Gentleman R, Carey V, Bates D *et al.* Bioconductor: open software development for computational biology and bioinformatics. *Genome Biol* 2004; **5**: R80.
20 Ishwaran H, Kogalur UB, Gorodeski EZ *et al.* High-dimensional variable selection for survival data. *J Amer Stat Assoc* 2010; **105**: 205–17.
21 Youden WJ. Index for rating diagnostic tests. *Cancer* 1950; **3**: 32–5.
22 Cancer Genome Atlas Research Network. Comprehensive genomic characterization defines human glioblastoma genes and core pathways. *Nature* 2008; **455**: 1061–8.
23 LeBlanc M, Crowley J. Relative risk trees for censored survival data. *Biometrics* 1992; **48**: 411–25.
24 Cordell HJ. Detecting gene–gene interactions that underlie human diseases. *Nat Rev Genet* 2009; **10**: 392–404.
25 Kawaguchi A, Iwadate Y, Komohara Y *et al.* Gene expression signature-based prognostic risk score in patients with primary central nervous system lymphoma. *Clin Cancer Res* 2012; **18**: 5672–81.

Supporting Information

Additional Supporting Information may be found in the online version of this article:

Fig. S1. Marginal plots for the six genes.

Fig. S2. Heat map for selected genes.

Fig. S3. Classification by cell-of-origin associated with survival.

Table S1. Quantitative PCR validation on survival-related genes.

doi: 10.1111/cas.12214